10484–10505 *Nucleic Acids Research, 2023, Vol. 51, No. 19* *Published online 11 September 2023*
https://doi.org/10.1093/nar/gkad733

RNF8 ubiquitylation of XRN2 facilitates R-loop resolution and restrains genomic instability in BRCA1 mutant cells

Rehna Krishnan[1,†], Mariah Lapierre[1,2,†], Brandon Gautreau[1,2], Kevin C.J. Nixon[1], Samah El Ghamrasni[1], Parasvi S. Patel[1,3], Jun Hao[1], V. Talya Yerlici[2], Kiran Kumar Naidu Guturi[1], Jonathan St-Germain[1], Francesca Mateo[4], Amine Saad[5], Arash Algouneh[1], Rebecca Earnshaw[1], Duan Shili[1], Alma Seitova[6], Joshua Miller[1], Negin Khosraviani[2], Adam Penn[1], Brandon Ho[7], Otto Sanchez[8], M. Prakash Hande[9], Jean-Yves Masson[10], Grant W. Brown[7], Moulay Alaoui-Jamali[5], John J. Reynolds[11], Cheryl Arrowsmith[1,3,6], Brian Raught[1,3], Miguel A. Pujana[4], Karim Mekhail[2], Grant S. Stewart[11], Anne Hakem[1,*] and Razqallah Hakem[1,2,3,*]

[1]Princess Margaret Cancer Centre, University Health Network, Toronto, Ontario M5G 1L7, Canada, [2]Department of Laboratory Medicine and Pathobiology, University of Toronto, Toronto, Ontario M5S 1A8, Canada, [3]Department of Medical Biophysics, University of Toronto, Ontario M5G 1L7, Canada, [4]Program Against Cancer Therapeutic Resistance (ProCURE), Catalan Institute of Oncology (ICO), Bellvitge Institute for Biomedical Research (IDIBELL), L'Hospitalet del Llobregat, Barcelona 08908, Catalonia, Spain, [5]Segal Cancer Centre and Lady Davis Institute for Medical Research, Departments of Medicine and Oncology, Faculty of Medicine, McGill University, Montreal, Quebec, Canada, [6]Structural Genomics Consortium, University of Toronto, Toronto, ON M5G 1L7, Canada, [7]Department of Biochemistry and Donnelly Centre, University of Toronto, Toronto, Ontario, Canada, [8]Ontario Tech University, 2000 Simcoe Street North Oshawa, Ontario L1G 0C5, Canada, [9]Department of Physiology, Yong Loo Lin School of Medicine, National University of Singapore, Singapore, [10]Genome Stability Laboratory, CHU de Québec Research Center, Oncology Axis; Department of Molecular Biology, Medical Biochemistry and Pathology; Laval University Cancer Research Center, 9 McMahon, Québec City, Québec G1R 2J6, Canada and [11]Institute of Cancer and Genomic Sciences, College of Medical and Dental Sciences, University of Birmingham, Birmingham, UK

Received May 09, 2023; Revised August 10, 2023; Editorial Decision August 12, 2023; Accepted August 24, 2023

ABSTRACT

Breast cancer linked with BRCA1/2 mutations commonly recur and resist current therapies, including PARP inhibitors. Given the lack of effective targeted therapies for BRCA1-mutant cancers, we sought to identify novel targets to selectively kill these cancers. Here, we report that loss of RNF8 significantly protects Brca1-mutant mice against mammary tumorigenesis. RNF8 deficiency in human BRCA1-mutant breast cancer cells was found to promote R-loop accumulation and replication fork instability, leading to increased DNA damage, senescence, and synthetic lethality. Mechanistically, RNF8 interacts with XRN2, which is crucial for transcription termination and R-loop resolution. We report that RNF8 ubiquitylates XRN2 to facilitate its recruitment to R-loop-prone genomic loci and that RNF8 deficiency in BRCA1-mutant breast cancer cells decreases XRN2 occupancy at R-loop-prone sites, thereby promoting R-loop accumulation, transcription-replication collisions, excessive genomic instability, and cancer cell death. Collectively, our work identifies a synthetic lethal interaction between RNF8 and BRCA1, which is mediated by a pathological accumulation of R-loops.

*To whom correspondence should be addressed. Tel: +1 416 634 8780; Email: rhakem@uhnres.utoronto.ca
Correspondence may also be addressed to Anne Hakem. Email: ahakem@uhnres.utoronto.ca
†The authors wish it to be known that, in their opinion, the first two authors should be regarded as Joint First Authors.

GRAPHICAL ABSTRACT

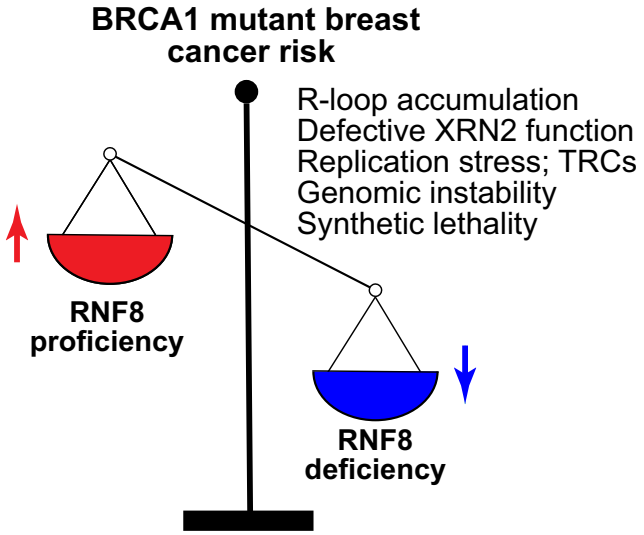

INTRODUCTION

Mutations in the *BRCA1* gene predispose for breast, ovarian and other cancer types (1,2). Women carriers of *BRCA1* mutations have a cumulative breast cancer risk of 72% by the age 80 (1). While the identification of PARP trapping being synthetically lethal for *BRCA1*-mutant tumor cells has led to the approval of several PARP inhibitors (PARPi) for clinical use, patients with *BRCA1*-mutant cancers tend to develop resistance to PARPi and to the platinum-based compounds currently used to treat these cancers (2). Drug resistance and the recurrence of the *BRCA1*-mutant cancers highlight the unmet need for novel therapeutic targets for these cancer patients.

BRCA1 is a multi-functional protein that plays a canonical role in the repair of DNA double-strand breaks (DSB) (3,4) by homologous recombination (HR). Growing evidence also supports a role for BRCA1 in transcriptional regulation, replication fork stability, and the resolution of DNA–RNA hybrids (R-loops) (5–7). R-loops form when the nascent RNA strand invades the DNA helix behind the transcribing RNA polymerase, forming a DNA–RNA hybrid and a displaced single-stranded DNA (8,9). In physiological contexts, R-loops regulate several cellular processes including DNA replication, transcription, and DNA damage repair (8,9). However, the accumulation of R-loops can cause transcription-replication collisions (TRCs) in S-phase, leading to elevated genomic instability and cell death (8–10).

The canonical function of BRCA1 in DSB repair depends on several signaling and repair factors and post-translational modifications of chromatin at the DNA break (3,11). RNF8 is critical for DSB signaling and repair (11–13). In response to DSBs, RNF8 ubiquitylates the linker histone H1 around the DNA breaks, thereby triggering a cascade of events culminating in the recruitment of factors necessary for the signaling and repair of these DSBs through HR (e.g. BRCA1) or the non-homologous end joining (e.g. 53BP1) pathways (3). Interestingly, prior studies indicate that while *BRCA1* mutations impair the HR-dependent DSB repair pathway, loss of 53BP1 in *BRCA1*-mutant cells restores HR repair and genomic stability and protects against mammary tumorigenesis associated with *BRCA1* mutations (14,15).

Given that 53BP1 deficiency protects from breast cancer associated with *BRCA1* mutations and the loss of RNF8 impairs 53BP1 recruitment to DSB-flanking sites (11), we examined the role of RNF8 in *BRCA1*-mutant breast cancer. Here, we show that RNF8 deficiency is synthetic lethal for human *BRCA1*-mutant breast cancer cells and protects *Brca1*-mutant preclinical mouse models from mammary tumorigenesis. Mechanistically, our data indicate that RNF8 deficiency in *BRCA1*-mutant breast cancer cells potentiates the levels of R-loops and replication stress, leading to TRCs, increased genomic instability and eventually cell death. This highlights the dependence of *BRCA1* mutated breast cancer cells on RNF8 for survival.

MATERIALS AND METHODS

Ethics approval

All procedures and studies involving mice were performed per the Princess Margaret Cancer Centre Animal Care Committee guidelines (Protocol numbers: 1223, 4805 and 2287).

Bioinformatic analysis

Gene expression levels were mapped to genes using RNA-seq of tumor and normal tissue samples obtained from The Cancer Genome Atlas (TCGA) for the following cancers: Bladder urothelial (BLCA), Breast invasive (BRCA), Cervical squamous cell, and Endocervical adenocarcinoma (CESC), Colon adeno (COAD), Head and neck squamous cell (HNSC), Kidney renal clear cell (KIRC), Liver hepatocellular (LIHC), Lung adenocarcinoma (LUAD), Lung squamous cell (LUSC), Pancreatic adenocarcinoma (PAAD), Prostrate adenocarcinoma (PRAD), Stomach adenocarcinoma (STAD) and Thyroid adenocarcinoma (THCA). Clinical and gene expression (RNA-seq fragments per kilobase of transcript per million mapped reads (FPKM) upper quartile normalized data from TCGA studies were obtained from the Genomic Data Commons portal (https://portal.gdc.cancer.gov). The HRD mutational signature was defined using the deconstructSigs (16) R package and MuTect somatic mutations in GDC. Individual-level data, including those relating to somatic mutations, were obtained with approval from the Data Access Committee (project 11689).

Mice

Rnf8$^{-/-}$ mice (17) (AS0574 strain) were crossed with *WAP-Cre*;*Brca1*$^{flox5\text{-}6,flox5\text{-}6}$ mice (18), which carry *loxP* sites flanking exons 5 and 6, to generate *Rnf8*$^{-/-}$;*WapCre;Brca1*$^{-/-}$ double mutant mice. Mice used in this study had a mixed 129/J × C57BL/6 genetic background and were genotyped by PCR as indicated (17,18). All female mice used in the survival cohort were allowed to progress through a minimum of four pregnancies to ensure proper Cre expression

and recombination of floxed alleles. Survival cohorts of female mice were monitored twice a week for over 500 days for mammary tumor onset by palpation and other tumor signs. All mice were housed in a pathogen-free mouse facility at the Princess Margaret Cancer Centre (PMCC). All procedures and studies involving mice were performed per the Princess Margaret Cancer Centre Animal Care Committee guidelines (Protocol numbers: 1223, 4805 and 2287).

Xenograft models

Logarithmically growing MDA-MB-436 shScr- or shRNF8-Tet-On cells were harvested, resuspended in PBS, and combined in a 1:1 ratio with Matrigel (Corning, 354248) at a concentration of 1.0 × 107 cells/ml. 100 μl of tumor cell suspensions were orthotopically injected into the inguinal fat pads of female NOD scid gamma (NSG) mice 6–7 weeks old. Tumor volume was measured externally using a digital caliper. Tumor volume was calculated as volume = (π × length × width 2)/6, where length represents the largest tumor diameter and width represents the diameter perpendicular to the length. Mice were given Dox at a concentration of 2mg/ml in their drinking water during experiments as indicated. To increase palatability, we supplemented the Dox-containing drinking water with 10% sucrose. Patient-derived xenograft experiments were performed using BRC#141 and IB-1 cells from breast cancer patient-derived xenograft models. Freshly collected xenograft tissue was minced using sterile scalpels and dissociated in a mixture containing DMEM/F-12/HEPES (GIBCO), 1 mg/ml collagenase (Roche), 100 U/ml hyaluronidase (Sigma), 25% BSA fraction V (GIBCO), 5 μg/ml insulin and 50 μg/ml gentamycin (GIBCO). Xenograft organoids were dissociated further using trypsin (GIBCO), dispase (StemCell technologies), and DNase (Sigma). Red blood cells were lysed by resuspending the cell pellet in a 1:4 solution of HF media (GIBCO): ammonium chloride (StemCell technologies). Following red blood cell lysis, cells were resuspended in HuMEC medium (GIBCO), divided into two equal aliquots, and transduced with lentiviral supernatant, either pLKO.shScr or pLKO.shRNF8, containing polybrene (8 μg/ml). The next day, single-cell suspensions were washed with PBS before being plated in triplicates in 96-well plates (day 0). Cell viability was monitored using CellTiter-Glo (Promega) at day 0 and then for an additional 10 days. ATP luminescence was normalized to day 0. RNF8 knockdown was verified on day 3 using real time quantitative reverse transcription PCR (RT-qPCR).

Cell lines and culture

Primary murine mammary epithelial cells were derived from double knockout mice and their single mutant and WT controls. SUM149PT cells (RRID:CVCL_3422) were cultured in Ham's F-12 nutrient mix (GIBCO, 11765054) supplemented with 10 mM HEPES, 1 μg/ml hydrocortisone (1 μg/ml), 5% FBS, insulin (5 μg/ml), penicillin and streptomycin. MDA-MB-436 (ATCC HTB-130), MDA-MB-231 (ATCC HTB-26), and HEK293FT cell lines (ATCC CRL-3249) were cultured in Dulbecco's modified Eagle's medium (DMEM) (Wisent, 319-005-CL) containing HEPES buffer, penicillin and streptomycin. DMEM was supplemented with 10% FBS (Wisent, 080-150) to support cell growth. PEO1 cells, obtained from R. Rottapel (Princess Margaret Cancer Centre, University Health Network, Toronto, Ontario, Canada), and Kuramochi (RRID:CVCL_1345) cells were cultured in RPMI (GIBCO) supplemented with 10% FBS, 5 × 10–5M 2-ME, 100 μ/ml penicillin and 100 μg/ml streptomycin (complete RPMI). All cell lines were passaged using 0.05% Trypsin–EDTA solution (Wisent, 325-542-EL) and maintained in a humidified 37°C, 5% CO_2 environment. Both MDA-MB-436 and SUM149PT cell lines carry mutations in the *BRCA1* gene, 5396 + 1G > A and c.2288delT, respectively (19). For virus generation, HEK293FT cells were transfected using calcium phosphate precipitation with constructs containing shRNA or sgRNA with psPAX-2 and pMD2.G. MDA-MB-231 cells were transduced with LentiCRISPR-V2 (Addgene #52961) containing a sgRNA targeting RNF8 (sgRNF8: 5′-CGGGGTCGAGTAGGCGATGG-3′) or a sgRNA targeting a non-coding region of chromosome 10 (sgCh10: 5′-CAATACACCCATAGTTGAGC-3′). We confirmed knockout clones using Western blotting. MDA-MB-231 cells were also transduced with pLKO.1-blast (Addgene #26655) containing an shRNA targeting human *BRCA1* (shBRCA1*;* TRCN0000244984: 5′-GAGTATGCAAACAGCTATAAT-3′) or an shRNA targeting a scrambled sequence (shScr: 5′-CCTAAGGTTAAGTCGCCCTCG-3′). MDA-MB-436, SUM149PT, Kuramochi and PEO1 cells were transduced with Tet-pLKO-Puro (Addgene #21915) encoding an shRNA targeting human *RNF8* (shRNF8.1: TRCN0000003438, shRNF8.2: TRCN0000003441) or shScr. Human XRN2 was knocked down in the MDA-MB-436 cells using pLKO.1-blast containing an shRNA targeting XRN2 (TRC293639 or shScr. For overexpression experiments, HEK293FT or MDA-MB-436 cells were transiently transfected using the calcium phosphate method. Human XRN2 was overexpressed using the p3xFlag-CMV-7-hXRN2 plasmid generously gifted to us from J Manley (Department of Biological Sciences, Columbia University, New York, New York). For rescue experiments, mouse *Rnf8* was overexpressed in MDA-MB-436 cells using the pINDUCER20 lentiviral construct (Addgene #44012). Western blotting was used to ensure proper knockdown or overexpression of all proteins.

DSB repair assays

To assess homologous recombination (HR), non-homologous end joining (NHEJ), and alternate end joining (a-EJ) repair efficiency, constructs containing HR or NHEJ (20) or alternative end-joining (a-EJ) (21) reporter cassettes were linearized with the I-SceI restriction enzyme (NEB) and transfected into *BRCA1*-mutant breast cancer cell lines using GenJet *in vitro* DNA transfection kit (SignaGen Laboratories). Red Fluorescent Protein (RFP) expressing construct was co-transfected as an internal control. Transfected cells were examined 48 h later by flow cytometry (BD Biosciences FACSCanto) and the levels of GFP and RFP expression were determined. FACS

Analyses were performed using FlowJo 10 software. Repair efficiencies of experimental samples were normalized relative to the control and represented as bar graphs.

Immunofluorescence

Immunofluorescence for sub-nuclear foci and IR-induced foci (IRIF) was performed in primary murine mammary epithelial cells and human cell lines. Cells were seeded onto coverslips and were treated with 8Gy γ-irradiation before fixation as indicated. Cells were fixed using 4% paraformaldehyde (Bioshop, PAR070) and permeabilized using 0.25% Triton-X 100 (Sigma, X100-5ML). After blocking in a buffer consisting of 5% FBS, 2.5% fish skin gelatin, 0.2% Triton X-100, and 0.5% BSA in 1X PBS, coverslips were incubated with primary antibodies at 4°C overnight. Coverslips were washed with 0.25% PBS-Tween20 (PBS-T). Secondary antibodies conjugated to Alexa Fluor 488 or 594 (1:1000; Life Technologies, A11008, A11037, A11001, A11032) were applied at room temperature for 1 h. while protected from light. Following washes, coverslips were counterstained with DAPI and mounted using Mowiol (Sigma, 81381). Primary antibodies used were anti-γH2AX (1:600; Millipore, 07-164; 05-636 JBW301), anti-53BP1 (1:1000; Bethyl, A300-272), anti-RNaseH1 (Proteintech Group, 15606-1-AP), and S9.6 (ATCC, HB-8730). For RNaseH1 overexpression experiments, cells were seeded and, after 24 h, transfected with pcDNA3-Empty or pcDNA3-RNase H1. 48 h post-transfection, cells were processed for immunofluorescence. Anti-RNaseH1 antibody was used to confirm the overexpression of RNaseH1.

DNA damage level of cells seeded onto coverslips was visualized using γH2AX immunofluorescence following 1h treatment with vehicle control, 2 μM flavopiridol (Selleckchem cat: S1230), 50 ng/ml actinomycin D (Sigma cat: A9415), or 500 nM APH (Sigma cat: A4487) and then processed for γH2AX immunofluorescence. Images were taken using a Lecia DM4000 B fluorescence microscope using 63× or 100× magnification. For the image quantifications, >100 cells were counted for all conditions from at least three independent experiments. ImageJ software (National Institutes of Health) was used to process and analyze raw image files. When scoring S9.6 nuclear intensity (mean grey intensity), nuclei in at least 5 random fields of view were measured per experiment. Microscope exposure settings were held constant within each experiment.

GFP-dRNH1 purification

GFP-tagged RNaseH1 (both WT and D210N) was transformed into Escherichia coli BL21(DE3)/Rosetta, cultured in media supplemented with kanamycin (50 μg/ml) and overnight induction by IPTG at 15°C. Induced bacterial cells (1L) were harvested and pelleted by centrifugation at 10 000 × g for 10 min. Bacterial pellets were resuspended on ice in 100 ml lysis buffer (50 mM Tris pH 8.0, 300 mM NaCl, 10% glycerol, 1 mM TCEP and EDTA-free protease inhibitor cocktail tablets) along with benzonase and lysed by sonication. Total cell lysate was centrifuged at 37 000 rpm for 60 min. The cleared supernatant was transferred to a new column containing 2ml of preequilibrated Ni–nitrilotriacetic acid Superflow beads and collected flowthrough. The columns were washed with 20 CV wash buffer (25 mM Tris pH 8.0, 300 mM NaCl, 10% glycerol, 1 mM TCEP, 15mM imidazole, 1 mM PMSF), followed by 20 CV of stringent wash buffer (25 mM Tris pH 8.0, 300 mM NaCl, 10% glycerol, 1mM TCEP, 30mM imidazole, 1 mM PMSF) and collected as wash. Samples were eluted five times with 2.5 CV elution buffer (25 mM Tris pH 8.0, 300 mM NaCl, 10% glycerol, 1 mM TCEP, 300 mM imidazole, 1 mM PMSF). The eluted samples were flash frozen and stored at −80°C. Purified GFP-RNaseH1 was quantified along with BSA standards and analyzed by Coomassie stained 4–12% SDS-PAGE to determine protein purity and concentrations. The protein stocks were aliquoted, stored at −80°C, and freshly thawed for each experiment.

GFP-dRNH1 immunofluorescence

Cells were seeded on 18mm coverslips. 48 h post seeding, cells were washed twice with 1 × PBS and fixed with 4% PFA for 10 min. The coverslips were washed twice with 1 × PBS, and permeabilized with 0.3% Triton X-100 in PBS. After two 1 × PBS washes, cells were blocked with 3% BSA in PBS for 30 min. RNaseH (1:50; New England Biolabs cat: M0297S) was diluted in 1X RNaseH buffer and incubated on coverslips for 3 h at 37°C. Cells were washed and blocked with 3% BSA in PBS for 30 min. Coverslips were then incubated with purified GFP-dRNH1 (1:2000; 0.188 mg/ml) in staining buffer for 1.5 h at 37°C. After washing thrice with PBST for 5 min, coverslips were counterstained with DAPI and mounted using MOWIOL. Slides were dried overnight prior to imaging and stored at 4°C in the dark.

Immunoprecipitation

MDA-MB-436 or HEK293FT cells were harvested, washed twice with ice-cold PBS, and centrifuged at 1500 RPM for 5 min at 4°C. Cell pellets were resuspended in a lysis buffer (50 mM Tris–HCl pH 7.5, 150 mM NaCl, 0.5% Triton-X100, and protease inhibitor cocktail tablets) and incubated on ice for 30 min. Cell debris was removed by centrifugation at 13200 RPM for 30 min at 4°C. 3 μg anti-RNF8 (Novus Biologicals, NBP1-77166), 2 μg Anti-Flag (Sigma, F3165), or control IgG antibody (Cell Signaling, 5415S) were added to the cleared lysate, and the mixture was rotated for 16 h at 4°C. Magnetic Protein G Dynabeads (Thermo Fisher, 10007D) were added and incubated for 2 h at 4°C. The beads were collected and washed with lysis buffer and eluted with 1× Laemmli SDS buffer. Immunoprecipitated proteins were detected using Western blot assay. RNF8, XRN2, and Flag-XRN2 were detected using the above primary antibodies, horseradish peroxidase-conjugated secondary antibodies to mouse (1:2000; Cell Signaling, 7076), and an enhanced chemiluminescence system (ECL) (Amersham).

Sample processing for liquid-chromatography-mass spectrometry

HEK293FT cells were transiently transfected with Flag-EV or Flag-RNF8. 48 h post-transfection, the cells were lysed, and pulldown was conducted using the IP protocol above. Following Flag-IP, beads were rinsed three times with the IP buffer and twice using NH_4HCO_3 (50mM, pH 8.3)/KCl (75 mM). Proteins were next eluted from the beads using NH_4OH (125mM). The eluates were lyophilized, reconstituted in NH_4HCO_3 (50 mM, pH 8.3) and digested with sequencing-grade trypsin (1 μg; Promega) overnight at 37°C on an end-to-end rotator. Samples were de-salted on C18 reverse-phase columns and lyophilized prior to LC–MS. The two experimental replicates allowed us to gauge the global reproducibility of the experiment. In addition, each replicate was analyzed as two technical replicates in the LC–MS to allow evaluation of the variations observed at the instrument-level. This was done not only to ensure quality control at the LC–MS level, but also to separate these variations, as minute as they may be, from variations observed between experimental replicates.

Liquid chromatography–mass spectrometry

Lyophilized samples were reconstituted in HCOOH (0.1%) and loaded on a pre-column (C18 Acclaim PepMapTM 100, 75 μm × 2 cm, 3 μm, 100 Å, Thermo Scientific) prior to chromatographic separation through an analytical column (C18 Acclaim PepMapTM RSLC, 75 μm × 50 cm, 3 μm, 100 Å, Thermo Scientific) by HPLC over a reversed-phase gradient (120-minute gradient, 5–30% CH_3CN in 0.1% HCOOH) at 225 nl/min on an EASY-nLC1200 pump in-line with a Q-Exactive HF mass spectrometer (Thermo Scientific) operated in positive ESI mode. An MS1 ion scan was performed at 60 000 fwhm followed by MS/MS scans (HCD, 15 000 fwhm) of the 20 most intense parent ions (minimum ion count of 1000 for activation). Dynamic exclusion (10 ppm) was set at 5 s.

LC–MS data processing

Raw MS files (.raw) were converted to .mzML using Proteowizard (v3.0.19311), then searched using X!Tandem (v2013.06.15.1) and Comet (2014.02 rev. 2) against human RefSeqV104 (containing 36113 entries). Search parameters specified a parent MS tolerance of 15 ppm and an MS/MS fragment ion tolerance of 0.4 Da, with up to two missed tryptic cleavages. No fixed modifications were set. Deamidation (NQ), oxidation (M), acetylation (protein N-term) and diglycine (K) were set as variable modifications. Search results were processed through the trans-proteomic pipeline (TPP v4.7), and proteins were identified with ≥2 unique peptides and an iProphet probability ≥0.9. For statistical analysis of interactors, a Bayesian false discovery rate (1% cut-off) was assigned using SAINT (v2.5.0) by comparing the spectral counts of each identified protein in a total of 18 negative control samples to counts in the Flag-RNF8 samples. For both the control and Flag-RNF8 samples, the top-2 counts across samples for each protein were used.

Chromatin immunoprecipitation

Cells were fixed in 1% formaldehyde followed by glycine neutralization. Cells were washed with ice-cold PBS and lysed with lysis buffer (50mM Tris pH 8.0, 2mM EDTA pH 8.0, 0.1% v/v NP40, 10% glycerol) supplemented with protease inhibitor. Nuclei were pelleted by centrifugation at 4°C and then lysed in nuclear lysis buffer (1% SDS, 10 mM EDTA pH 8.0 and 50 mM Tris pH 7.5). Chromatin was sonicated to produce an average fragment length of 250–400 bp. For each IP, 50 μl of chromatin was diluted 10 times in IP dilution buffer (0.01% SDS, 1.1% TritonX-100, 1.1 mM EDTA, 20 mM Tris–HCl pH 8.0, 167 nM NaCl) and incubated with 3 μg anti-XRN2 (Bethyl, A301-103A), 4 μg anti-SETX (Bethyl, A301-105A) or an equivalent amount of control IgG overnight with rotation at 4°C. The next day, 30 μl of pre-washed Dynabeads were added to each sample and incubated for 2 h. at 4°C with rotation. Beads were washed using rotation, and the immunoprecipitated DNA eluted as previously described (22). DNA samples were reverse cross-linked and treated with RNaseA and proteinase K (PK). DNA was purified using a GeneAid PCR purification kit (GeneAid Biotech, DFH100, DFH300) as per the manufacturer's instructions. Real-time quantitative PCR (RT-qPCR) was run in triplicate using an ABI PRISM 7900HT Sequence Detection System or Bio-Rad CF96. The primers used are listed in Supplementary Table S2.

Drip

shScr- and shRNF8-Tet-On MDA-MB-436 cells were pelleted and lysed using a DNA lysis buffer (10 mM Tris–HCl, 1 mM EDTA, 10% SDS) supplemented with PK and incubated overnight at 37°C. Genomic DNA was precipitated using 5 M NaCl followed by isopropanol. The DNA was washed with 70% ethanol and resuspended in 1× TE (10 mM Tris–HCl, 1mM EDTA). DNA concentration was measured using a NanoDrop One Microvolume UV-vis spectrophotometer (ThermoFisher). Sixty μg of genomic DNA was digested using HindIII, EcoRI, XbaI & BamHI restriction enzymes (NEB) overnight at 37°C. The following day, the DNA sample was divided into equal aliquots, and 30 μg of DNA were treated with RNaseH (NEB) for 4 h at 37°C as an S9.6 antibody specificity control. Phenol/chloroform extraction and ethanol precipitation were used to purify the DNA. Per IP, 10 μg of digested DNA was used along with antibodies against S9.6 or IgG. The DNA/antibody mixture was rotated overnight at 4°C. The following day, the IP samples were added to equilibrated Dynabeads and rotated for 2–4 h at 4°C. After rotating, the beads were washed with IP buffer and were incubated with PK diluted in PBS for 3 h at 56°C. The DNA was purified from the beads using phenol/chloroform extraction followed by ethanol precipitation. The resulting DNA was resuspended using 1× TE and was analyzed using qPCR. The primers used are listed in Supplementary Table S2.

DRIP-sequencing library preparation and analysis

DNA–RNA hybrids isolated using the method outlined above were submitted for library preparation and

sequencing to Novogene. NEB Next Ultra II DNA Library preparation kit was used to prepare the library. Following quality control, fragments were repaired and dA-tailed. The DNA fragments with A tail were ligated to sequencing adaptors. The final DNA library was obtained by size selection and PCR amplification. After the construction of the library, the initial quantification was done with Qubit 2.0, and the library is diluted to 1 ng/l. Then the insertion size of the library was detected with NGS3K. If meeting the expectation, the accurate concentration of the library was quantified by qPCR (library effective concentration > 2 nM) to ensure the accurate molar amount that will be pooled for sequencing. After library quality control, sequencing was performed for different libraries according to the concentration and the demand of data amount on Illumina NovaSeq platform (NovaSeq 6000). RNF8 DRIP-Seq data can be accessed using the following credentials: Accession: GSE202723; Reviewer token: kbsjkyagxhsntyn.

Raw reads were trimmed using trim galore! (v. 0.6.6) and mapped to hg38 using Bowtie2 (23) (v. 2.2.6). Low quality and multimapping reads were removed using samtools (v. 1.14) and duplicate reads were marked and removed using PICARD (GATK tools v. 2.10.9). Peaks were called using MACS2 (24) (v. 2.2.7.1) with the -q flag indicating and FDR cutoff of 0.01. Reproducible peaks from replicates within each condition were identified using the irreproducible discovery rate (IDR) method (25) using the default parameters. DRIP signal coverage files were generated using deeptools (26) (v. 3.5.1) bamCompare to normalize samples to read depth and calculate the $\log_2$ratio of IP signal over input. Average signal was calculated using bigwigCompare or wiggletools mean (v. 1.2.11) and average DRIP coverage was calculated for active gene bodies (±10 kb) using computeMatrix scale-regions or active gene transcription termination sites (TTS; +/- 3kb) using computeMatrix reference-point. Metagene profiles and average DRIP signals were plotted using a custom script and ggplot2 in R (v. 4.0.2). Reproducible peaks were annotated to the human genome using the Bioconductor packages ChIPseeker (v. 1.32.0) and TxDb.Hsapiens.UCSC.hg38.knownGene. R-loop positive ('R-loop + ve') genes were defined as expressed protein-coding genes (TPM > 0) with peaks annotated to the transcription termination sites (TTS) in either shScr (3822 genes) or shRNF8 (3314 genes) samples. Expression of R-loop +ve genes were compared to expressed protein-coding genes without peaks annotated to the TTS (R-loop negative; 'R-loop-ve') using a Wilcoxon Rank-Sum test.

RNA-sequencing and analysis

Total RNA from MDA-MB-436 cells transduced with scrambled or RNF8 shRNA was extracted using the RNeasy kit (Qiagen), and RNA quality was assessed by Agilent 2100 Bioanalyzer (Agilent Technologies). Total RNA was submitted for library preparation and sequencing to Novogene. Raw reads were trimmed using trim galore! (v. 0.6.6; https://www.bioinformatics.babraham.ac.uk/projects/trim_galore/) and mapped to hg38 using STAR (27) (v. 2.7.9a). Low quality and multimapping reads were removed using samtools (28) (v. 1.14) and reads were counted to exonic features using featureCounts (29) (subread v. 2.0.1). Raw gene counts were normalized to transcripts per million (TPM) and protein coding genes with an average TPM > 0 across all samples were identified as active genes and used for downstream analyses. RNF8 RNA-Seq data can be accessed using the following credentials: Accession: GSE202723; Reviewer token: kbsjkyagxhsntyn.

DNA fibre assay

MDA-MB-436 shRNF8- or shScr-Tet-On cell lines were incubated with media containing either 1 μM Dox or DMSO for 4 days before DNA fibre analysis. Cells were pulse-labelled with 25 μM CldU for 20 min, washed with medium, and subsequentially pulse-labelled with 250 μM IdU for an additional 20 min. Cells were harvested by trypsinization and washed in PBS. 10000 cells were then lysed directly onto glass microscope slides using spreading buffer (200 mM Tris–HCl pH 7.5, 50 mM EDTA, 0.5% SDS), and DNA fibres were allowed to spread down the slide by gravity. DNA fibres were fixed in methanol:acetic acid (3:1 ratio), denatured with 2.5M HCl, and immunostained. CldU was detected using rat anti-Bromodeoxyuridine (BrdU) (1:750; Abcam, ab6326), and IdU was detected using mouse anti-BrdU (1:750; BD Biosciences, 347583). Slides were fixed in 4% paraformaldehyde and incubated with secondary antibodies conjugated to Alexa Fluor 594 or Alexa Fluor 488 (Life Technologies). Labelled DNA fibres were visualized using a Nikon Eclipse Ni microscope with NIS-Elements software (Nikon Instruments), and images were captured using 60× oil-immersion objectives and analysed using ImageJ software. Tract lengths were measured using ImageJ, and pixel length values were converted into μM using the scale bars created by the microscope.

SA-β-gal staining

β-gal activity at pH 6.0 was used to monitor senescence levels *in vitro*. Staining was performed using a commercially available kit (Cell Signaling Technologies, 9860S) as per the manufacturer's instructions.

Clonogenic assays

Cells were seeded in 6 cm dishes as indicated in figure legends. Cells were allowed to grow under experimental conditions for 14–28 days before methanol fixation and crystal violet staining. In PARPi sensitivity assays, olaparib (Selleckchem, S1060) was used at a concentration of 1–2 μM for MDA-MB-231 cells, and the media was changed every 4 days to maintain drug concentration throughout the experiment. The MDA-MB-436 cells were treated with 5–10 nM as indicated. Data from treated samples were normalized to untreated (DMSO) conditions. Images of representative dishes were captured using a Canon LiDE scanner and brightened using Adobe Illustrator. Experiments were performed in technical triplicates.

In vivo ubiquitylation assay

IP was performed for XRN2 using MDA-MB-436 and MDA-MB-231 cells as previously described. The cell lysates

were immunoprecipitated with an anti-XRN2 antibody (1:500; Santa Cruz, sc-365258). The ubiquitin conjugates were detected by Western blot analysis as previously described using anti-Ubiquitin antibodies (1:000; Cell Signaling, P4D1).

In vitro ubiquitination assay

Recombinant RNF8 (0.3 μg), recombinant XRN2 (2 μg), UBE1 (0.05 μg; E1), UBE2E2 (0.2 μg; E2), HA-Ub (5 μg) were mixed, and the reactions were incubated at 30°C for 90 minutes in buffer containing 50 mM Tris/HCl (pH 7.5), 5 mM $MgCl_2$, 5mM ATP and 2 mM DTT. Ubiquitylation was examined using Western blotting and anti-ubiquitin antibody (1:000; Cell Signaling, P4D1).

Western blotting

Cell extracts were prepared in RIPA buffer (10 mM Tris–HCl pH 8.0, 1 mM EDTA, 0.5 mM EGTA, 1% Triton X-100, 0.1% sodium deoxycholate, 0.1% SDS and 140 mM NaCl) and sonicated to release DNA-bound proteins. Primary antibodies used were anti-RNF8 (Santa Cruz sc-271462, 1:500), anti-BRCA1 (Millipore cat: MS110, 1:100), anti-phospho-S428 ATR (Cell Signaling 2853T, 1:1000), anti-ATR (Cell Signaling 2790S, 1:1000), anti-RPA32 (Bethyl A300-081A, 1:1000), anti-phospho-S33 RPA32 (Bethyl A300-426A, 1:1000) and anti-β-ACTIN (Santa Cruz sc-47778, 1:5000).

Proximity ligation assay (PLA)

Cells were seeded on 12 mm coverslips. 48 h post-seeding, cells were treated with cold 0.5% NP-40 for 4 min on ice. Cells were then fixed with 1% PFA/PBS for 15 min and washed three times with PBS. The coverslips were blocked for 1 h at room temperature with 2% BSA in PBS. Cells were then incubated in primary antibody overnight at 4°C (1:500 anti-Pol II (Santa Cruz cat: sc-17798) alone; 1:500 anti-PCNA (Santa Cruz cat: sc-7907) alone; or 1:500 anti-Pol II with 1:500 anti-PCNA). After the incubation, coverslips were washed two times with wash buffer A and incubated in a mixture of PLA probe anti-mouse minus and PLA probe anti-rabbit plus (Sigma cat: DUO92101) for 1 h at 37°C. The Duolink *in Situ* detection reagents (Sigma cat: DUO92008) were used to perform the PLA reaction according to the manufacturer's instructions. Cells were counterstained with DAPI and fixed on a glass slide using MOWIOL. All immunofluorescence images were taken and analyzed using a Lecia DM4000 B fluorescence microscope using 100× magnification as indicated in figure legends. For the image quantifications, >100 cells were counted for all conditions from at least three independent experiments.

EU incorporation assay

EU incorporation assays were performed using the Click-iT RNA Alexa Fluor 594 Imaging Kit (Invitrogen) according to the manufacturer's instructions. Cells were incubated with 1 mM EU for 30 min, fixed with 4% PFA for 15 min at room temperature, permeabilized with 0.3% Triton X-100 for 15 min, and the Click-iT reaction was performed. DNA was counterstained with DAPI, and images were acquired using a Lecia DM4000 B fluorescence microscope.

Statistical analysis

Graphs are depicted as mean ± SEM unless otherwise indicated. Experiments were performed for at least three biological replicates. All statistical analyses were performed using GraphPad Prism 9 and the specific statistical tests used are indicated in the figure legends. *n* represents the number of biological replicates that were performed. *P* values <0.05 were considered statistically significant. * $P < 0.05$, ** $P < 0.01$, *** $P < 0.001$ and **** $P < 0.0001$.

RESULTS

RNF8-deficiency protects against *BRCA1* mutant breast cancer and restrain *in vitro* and *in vivo* growth of *BRCA1* mutant cancer cells

The E3 ubiquitin ligase RNF8 propagates the DSB signaling cascade critical for repairing DNA damage and maintaining genomic stability (13). Given the importance of RNF8 in HR-mediated DSB repair (13,30), we examined the effect of Rnf8 loss on mammary tumorigenesis associated with *Brca1* mutations. We generated mouse models deficient for Rnf8, Brca1, or both proteins in the mammary epithelium. Mouse models with mutations in *Brca1* in mammary epithelial cells have a high risk of developing mammary tumors (18,31), and while $Rnf8^{-/-}$ mice develop lymphomas, they also display an increased risk for mammary tumorigenesis (17,32). In order to examine the effect of dual loss of Brca1 and Rnf8 on breast cancer, we crossed mice that carry a *Brca1*-null mutation in mammary epithelial cells(18) (*WAP-Cre*;$Brca1^{flox5\text{-}6,flox5\text{-}6}$; referred to as *WAP-Cre*;$Brca1^{-/-}$) with $Rnf8^{-/-}$ mice (17), and generated cohorts of double mutant ($Rnf8^{-/-}$;*WAP-Cre*;$Brca1^{-/-}$), single mutant ($Rnf8^{-/-}$ or *WAP-Cre*;$Brca1^{-/-}$) and wildtype (*WT*) females. After 17 months monitoring these cohorts of female mice, we observed an elevated risk for mammary tumorigenesis in the cohort of *WAP-Cre*;$Brca1^{-/-}$ females, with over half of these females succumbing to mammary tumors (Figure 1A). While $Rnf8^{-/-}$ females also developed mammary tumors, the frequency was significantly lower than in *WAP-Cre*;$Brca1^{-/-}$ female littermates (Figure 1A). Contrasting with the elevated risk of mammary tumorigenesis in *Brca1*-mutant females, $Rnf8^{-/-}$;*WAP-Cre*;$Brca1^{-/-}$ females were remarkably protected from developing spontaneous mammary tumors, and there was no difference in mammary tumor-free survival when comparing double-mutant females with RNF8 mutant or wildtype controls (Figure 1A). These data revealed that loss of Rnf8 significantly protects against mammary tumorigenesis associated with *Brca1* mutations.

Next, we explored the role of RNF8 in human cancer using the provisional TCGA (The Cancer Genome Atlas) datasets and compared RNF8 expression in a panel of 13 different cancers with their normal tissue counterparts. Compared to corresponding normal tissue, *RNF8* was significantly overexpressed in six different cancers, including breast cancer (Supplementary Figure S1a). Given

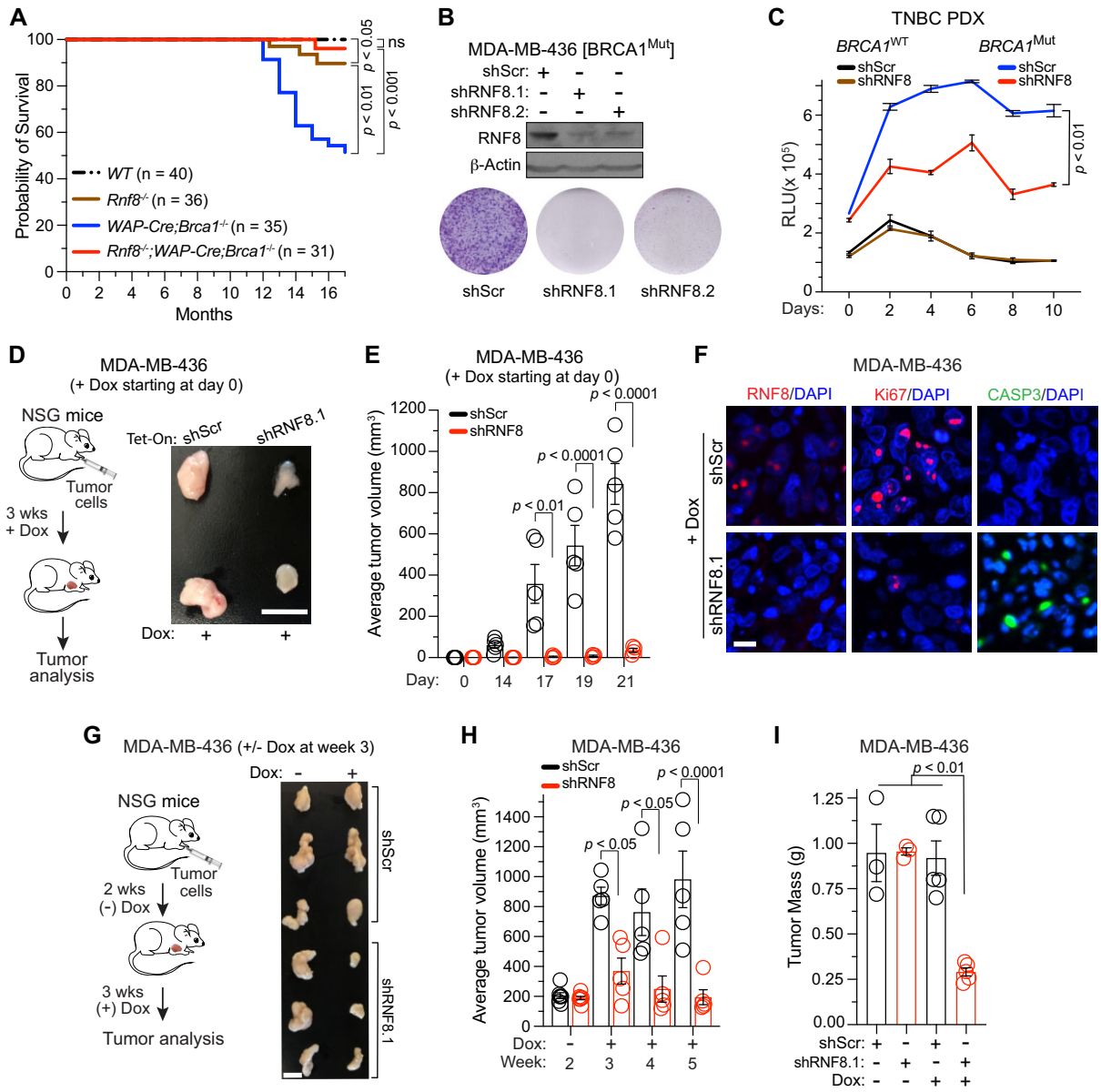

Figure 1. Increased expression of RNF8 in HRD breast cancer and its deficiency markedly protects mouse models of *Brca1* mutation from mammary tumorigenesis. (**A**) Graph showing mammary tumor-free survival of mice with the cohorts of WT ($n = 40$), *Rnf8*$^{-/-}$ ($n = 36$), *Wap-Cre Brca1*$^{-/-}$ ($n = 35$), and *Rnf8*$^{-/-}$*; Wap-Cre Brca1*$^{-/-}$ ($n = 31$). (**B**) Western blot (WB) analysis of the indicated MDA-MB-436 cells (upper panel). MDA-MB-436 cells transduced with Tet-On shRNF8 and shScr were treated with Dox for 7 days (BRCA1^{Mut}: BRCA1 mutant). β-Actin was used as a loading control. The indicated Dox-induced MDA-MB-436 cells (100 000) were seeded per 6 cm dish, grown for 14 days, and stained with crystal violet (bottom panel). (**C**) Relative growth of primary cultures of the indicated PDX cells expressing mutated (IB-1) and WT (BRC#141) *BRCA1* ($n = 3$). The chart depicts relative light units (RLU) detected for each primary xenograft, measured daily for 10 days. (**D**) A schematic of the experimental setting used to examine the effect of RNF8 deficiency on *in vivo* growth of xenografts of *BRCA1*-mutant TNBC cells and representative images of the indicated MDA-MB-436 mammary tumors resected 3 weeks post-injection (n = 5 per condition; bar = 1 cm). (**E**) Graph depicting changes in tumor volume over 21 days as in (D). (**F**) Tumors in (D) were sectioned and immunostained with RNF8, Ki67, and cleaved CASP3 antibodies. Representative images are shown (bar = 12.5 μm). (**G**) A schematic of the experimental setting used to examine *in vivo* effects of RNF8 depletion on established *BRCA1*-mutant tumors. MDA-MB-436 cancer cells were injected into NSG mice**,** and tumors were allowed to grow for two weeks before giving all cohorts of mice Dox in drinking water for another 3 weeks. Representative images 5 weeks post transplantation are shown for the indicated MDA-MB-436 mammary tumors resected from NSG mice ($n > 4$ per condition; bar = 1 cm). (**H, I**) Tumor volumes and mass from mice in (G) were monitored for 5 weeks. Graphs are depicted as mean ± SEM unless otherwise indicated. Data were analyzed using the log-rank test (A), two-tailed, paired Student's *t*-test (C), two-way ANOVA with Sidak's multiple comparisons test (E, H), and one-way ANOVA with Tukey's multiple comparisons test (I). ns: not significant. WT: wildtype. Mut: mutant.

that *BRCA1* mutations are associated with defects in HR-mediated repair of DSBs (3,4), we examined RNF8 expression in HR-deficient or proficient breast cancers. Homologous recombination deficiency (HRD) occurs when genes that regulate the HR-dependent repair pathway are mutated. HRD has been linked with a specific pattern of genome-wide mutations (mutational signature 3), which can predict biallelic inactivation of *BRCA1* and germline or somatic alterations of HR-related genes (33,34). Interestingly, we observed high RNF8 expression in HRD breast tumors (mutational signature 3-positive) compared to signature 3-negative tumors (Supplementary Figure S1b). Similarly, in mutational signature 3 positive HRD breast cancers we observed higher expression of RNF168 and RAD51, factors that function downstream of RNF8 in the DSB repair pathway (Supplementary Figure S1b). Furthermore, examination of signature 3 scores in TCGA primary breast tumors classified into tertiles of *RNF8* expression identified a significant correlation between high signature 3 scores and elevated expression of *RNF8* (Supplementary Figure S1c). Given that *BRCA1* mutations predispose for the development of triple-negative breast cancer (TNBC) (1), we next examined signature 3 scores in TCGA within TNBC classified into tertiles of *RNF8* expression. We observed that *RNF8* expression was elevated in TNBC displaying mutational signature 3 (Supplementary Figure S1d). Notably, the elevated expression of RNF168 and RAD51 positively correlated with high signature 3 scores in TCGA BRCA, but this correlation was not significant in TCGA BRCA TNBC (Supplementary Figure S1c,d). Collectively, these data reveal that RNF8 is overexpressed in several cancers, including breast cancer, and the levels of RNF8 expression are higher in HRD breast tumors including TNBC compared to HR-proficient tumors.

To examine the clinical relevance of increased RNF8 expression in HRD breast tumors, we performed *in vitro* colony-forming assays and examined the growth of *BRCA1/2*-mutant breast and ovarian cancer cells transduced with Doxycycline (Dox) -inducible shRNA for RNF8 (shRNF8) or scrambled sequence (shScr). We observed that RNF8 depletion significantly impaired the growth of BRCA1 mutant MDA-MB-436 TNBC cells and BRCA2 mutant Kuramochi ovarian cancer cell line (Figure 1B and Supplementary Figure S2a). To further examine the effect of RNF8 knockdown on the growth of human *BRCA1*-mutated breast tumor cells, we used patient-derived xenografts (PDX) derived from a breast cancer patient harboring a deleterious *BRCA1* germline mutation (IB-1) and a breast cancer patient carrying wildtype *BRCA1* alleles (BRC#141). We transduced cells from these PDXs with shRNF8 or shScr and assessed RNF8 knockdown using RT-PCR (Supplementary Figure S2b). We then examined the viability of shRNF8 and shScr PDX cells using an ATP luminescence assay. Whilst RNF8 depletion did not alter the viability of breast cancer cells proficient for BRCA1 (BRC#141), it significantly reduced the viability of *BRCA1*-mutatant IB-1 PDX cells (Figure 1C).

Given that RNF8 loss resulted in defective *in vitro* growth of BRCA1-deficient TNBC cells, we explored the effect of RNF8 depletion on the *in vivo* growth of these cells. We transplanted Dox-inducible shRNF8 and shScr MDA-MB-436 cells in the mammary fat pads of immunocompromised NOD scid gamma (NSG) mice. To induce expression of the shRNA, we provided each cohort of mice with drinking water supplemented with Dox for 21 days starting immediately following cell injection (Figure 1d). Consistent with the impact of RNF8 knockdown on PDX tumor cell growth, MDA-MB-436 cells depleted of RNF8 formed markedly smaller tumors compared to shScr transduced controls (Figure 1D, E). Immunohistochemistry (IHC) staining of shRNF8 MDA-MB-436 tumors from NSG mice that were given Dox immediately post-transplantation (Figure 1D), validated the knockdown of RNF8, and revealed decreased proliferation (Ki67 marker) and increased apoptosis (cleaved CASP3) (Figure 1F and Supplementary Figure S2c,d) compared to NSG mice bearing shScr MDA-MB-436 xenografts.

Next, we examined whether RNF8 depletion could halt the growth of established *BRCA1*-mutant breast tumors *in vivo*. Thus, we conducted a set of experiments in which shRNF8 and shScr MDA-MB-436 xenografts were first allowed to grow in the absence of Dox for two weeks post-transplantation before giving the mice drinking water with or without Dox for the following three weeks (Figure 1g). No significant differences in tumor volume or mass were observed between shRNF8 and shScr MDA-MB-436 tumor bearing mice that were not given Dox-containing drinking water for 3 weeks (Figure 1G–I). Mice given Dox-containing drinking water at week three post-xenotransplantation of shScr MDA-MB-436 cells developed tumors with a comparable volume and mass compared to their control cohort of mice not given Dox, yielding tumors of a comparable volume and mass (Figure 1G–I). In contrast, RNF8 knockdown tumors showed significantly reduced *in vivo* growth compared to all other cohorts (Figure 1G–I). Examination of the tumor volume of the cohort of mice xenografted with RNF8-depleted MDA-MB-436 cells indicated no significant difference of their tumor volumes at the two-week time point compared to the five-week endpoint (Figure 1G–I).

Given the sensitivity of *BRCA1*-mutant cells to PARPi (2,35,36), we examined the effect of RNF8 deficiency on the response of MDA-MB-436 cells to the PARPi olaparib. We observed a higher olaparib sensitivity of RNF8 depleted BRCA1 mutant MDA-MB-436 cells compared to their shScr controls (Supplementary Figure S2e,f). To validate this finding, BRCA1 proficient MDA-MB-231 TNBC cells and their isogenic counterparts deficient for RNF8 (sgRNA RNF8: sgRNF8), BRCA1 (shBRCA1) or both proteins, along with controls (sgCh10 and shScr), were also examined for their sensitivity to PARPi. MDA-MB-231 cells deficient for either RNF8 or BRCA1 displayed increased sensitivity to olaparib compared to controls (Supplementary Figure S2g, h). Consistent with data from MDA-MB-436 cells (Supplementary Figure S2e,f), deficiency of RNF8 further sensitized BRCA1-depleted MDA-MB-231 cells to olaparib (Supplementary Figure S2g, h). Together, these findings identify a dependence on RNF8 for the *in vitro* and *in vivo* growth of *BRCA1*-mutant cancer cells. Furthermore, our results indicate that RNF8 deficiency hyper-sensitizes *BRCA1*-mutant TNBC cells to PARP inhibition.

RNF8 deficiency increases genomic instability and senescence in *BRCA1*-mutant cells

The above results clearly indicate the critical function of RNF8 in *BRCA1/2*-associated tumorigenesis. Interestingly, RNF8 plays an important role in the recruitment of 53BP1 to DSB-flanking sites (11,37) and the loss of 53BP1 protects *Brca1*-mutant mouse models from mammary tumorigenesis (14), hence we used MDA-MB-231 cells deficient for RNF8, BRCA1 or both (Figure 2a), and examined the effect of RNF8 deficiency on the formation of 53BP1 foci in *BRCA1*-mutant human breast cancer cells. Six hours post-irradiation (IR), immunofluorescence staining of BRCA1-deficient MDA-MB-231 cells showed no significant defect in 53BP1 recruitment to DSB-flanking sites compared to BRCA1-proficient controls (Supplementary Figure 3A, B). However, as expected IR-induced 53BP1 foci formation was severely impaired in MDA-MB-231 cells deficient for RNF8 alone or both RNF8 and BRCA1 (Supplementary Figure 3A, B), confirming that loss of RNF8 in BRCA1 deficient cells compromised the integrity of the ubiquitin-dependent DNA damage response.

Considering the importance of RNF8, BRCA1, and 53BP1, in maintaining genomic stability (3,11) and that the loss of RNF8 impaired 53BP1 foci formation in MDA-MB-231 cells, we examined the ability of these cells to form γH2AX foci, a marker of DNA damage. We observed elevated levels of spontaneous DNA damage in MDA-MB-231 cells deficient for both RNF8 and BRCA1 compared to their isogenic cells deficient for either RNF8 or BRCA1 (Figure 2A and B). To validate this observation, we depleted RNF8 in the *BRCA1*-mutant TNBC cell lines (MDA-MB-436 and SUM149PT), and *BRCA2*-mutant ovarian cancer cell lines (Kuramochi and PEO1) and examined their level of DNA damage. Notably, we observed that depletion of RNF8 in cell lines with mutations in either *BRCA1 or BRCA2* significantly increased the level of spontaneous DNA damage (Figure 2C, D and Supplementary Figure S3c–f) as well as the ability to resolve IR-induced DNA damage at late timepoints post-irradiation (Figure 2C). Importantly, a similar phenotype was observed in the *Rnf8* and *Brca1* double-knockout primary murine mammary epithelial cells (MECs) when compared to single knockout or WT control MECs (Figure 2E and Supplementary Figure S3g). To further support the role of RNF8 in maintaining genomic stability in *BRCA1*-mutant cells, we transduced shRNF8 MDA-MB-436 cells with a Dox-inducible lentiviral vector expressing mouse *Rnf8* that is insensitive to the shRNA targeting human *RNF8* (Supplementary Figure S3h). Crucially, expression of mouse Rnf8 significantly reduced the elevated levels of DNA damage observed in shRNF8 MDA-MB-436 cells (Supplementary Figure S3i, j), further supporting the role of RNF8 in maintaining genomic stability in *BRCA1* mutant breast cancer cells.

To further determine the effect of RNF8 deficiency on the capacity of *BRCA1* mutant TNBC cells to repair DSBs, MDA-MB-436 cells with or without RNF8 knockdown were analyzed using well characterized I-SceI based DSB repair reporter assays (20,21) (Supplementary Figure S4). We found that RNF8 depletion in MDA-MB-436 cells significantly decreased the efficiency of HR and non-homologous DNA end joining (NHEJ) mediated DSB repair, whereas no significant change was observed in the alternative end-joining (a-EJ) DSB repair (Figure 2F). DNA content analysis using Hoechst staining of RNF8-depleted MDA-MB-436 cells revealed an increase in the sub-G1 population indicative of cell death, as well as elevated frequency of polyploidy (Figure 2g). These results highlight the importance of RNF8 in DSB repair and genome stability in *BRCA1*-mutant cells.

Impaired genomic stability can induce cellular senescence (38). Therefore, using the senescence-associated β-galactosidase staining (SA-β-gal) (38), we assessed the level of senescence in *Rnf8* and *Brca1* double-mutant primary MECs and RNF8 depleted human cancer cells with and without BRCA1. MECs lacking RNF8 and BRCA1 exhibited increased SA-β-gal positivity and were more enlarged and flattened than the single mutants and WT controls (Figure 2h and Supplementary Figure S5a). This was recapitulated in the RNF8-deficient MDA-MB-436 and SUM149PT cells, and MDA-MB-231 cells deficient for both RNF8 and BRCA1 (Supplementary Figure S5b-d and 5i,j). Interestingly, *Rnf8* and *Brca1* double-mutant MECs exhibited reduced proliferation, as judged by Ki67 staining, relative to *Rnf8* or *Brca1* single knockout MECs (Supplementary Figure S5e). Furthermore, RNF8 depleted MDA-MB-436 cells also displayed a reduction in Ki67 staining, increased expression of the senescence markers $P16^{INK4}$ and $P21^{CIP1}$ and an elevated percentage of apoptotic cells compared to shScr controls (Supplementary Figure S5f-h and Supplementary Table S1). Collectively, these data reveal that RNF8 deficiency in *BRCA1*-mutant cells impairs multiple DSB repair pathways and promotes genomic instability, senescence, and cell death.

RNF8 deficiency increases transcription dependent DNA damage and R-loop accumulation

RNF8 plays a critical role in the ubiquitin-dependent response to DSBs and acts as a positive regulator of the repair signaling cascade (11–13). Prior studies indicated that depletion of RNF8 and RNF168 partially reverses the ATM-dependent transcription silencing at the sites of DSBs (39,40). As such, RNF8 mediated DSB repair might prevent DSB-induced RNAPII stalling, thereby reducing conflicts with replication machinery. Hence, we examined the global transcription activity in shRNF8 MDA-MB-436 cells and their shScr controls by quantifying nascent RNA synthesis based on the incorporation of the modified RNA precursor 5-ethynyluridine (EU). Interestingly, RNA synthesis was found significantly higher in RNF8-depleted cells when compared to controls, indicating aberrant transcriptional regulation in cells lacking RNF8 and BRCA1 (Supplementary Figure S6a).

R-loops are transcriptional by-products that function as crucial regulatory intermediates in different cellular processes (8,9). However, the presence of excessive DNA–RNA hybrid-containing structures can also promote DNA damage and disease (8,9). While BRCA1 is important for HR-mediated DSB repair and replication fork stability (6,41), BRCA1 also interacts with the helicase Senataxin (SETX) to facilitate the resolution of R-loops associated with DNA

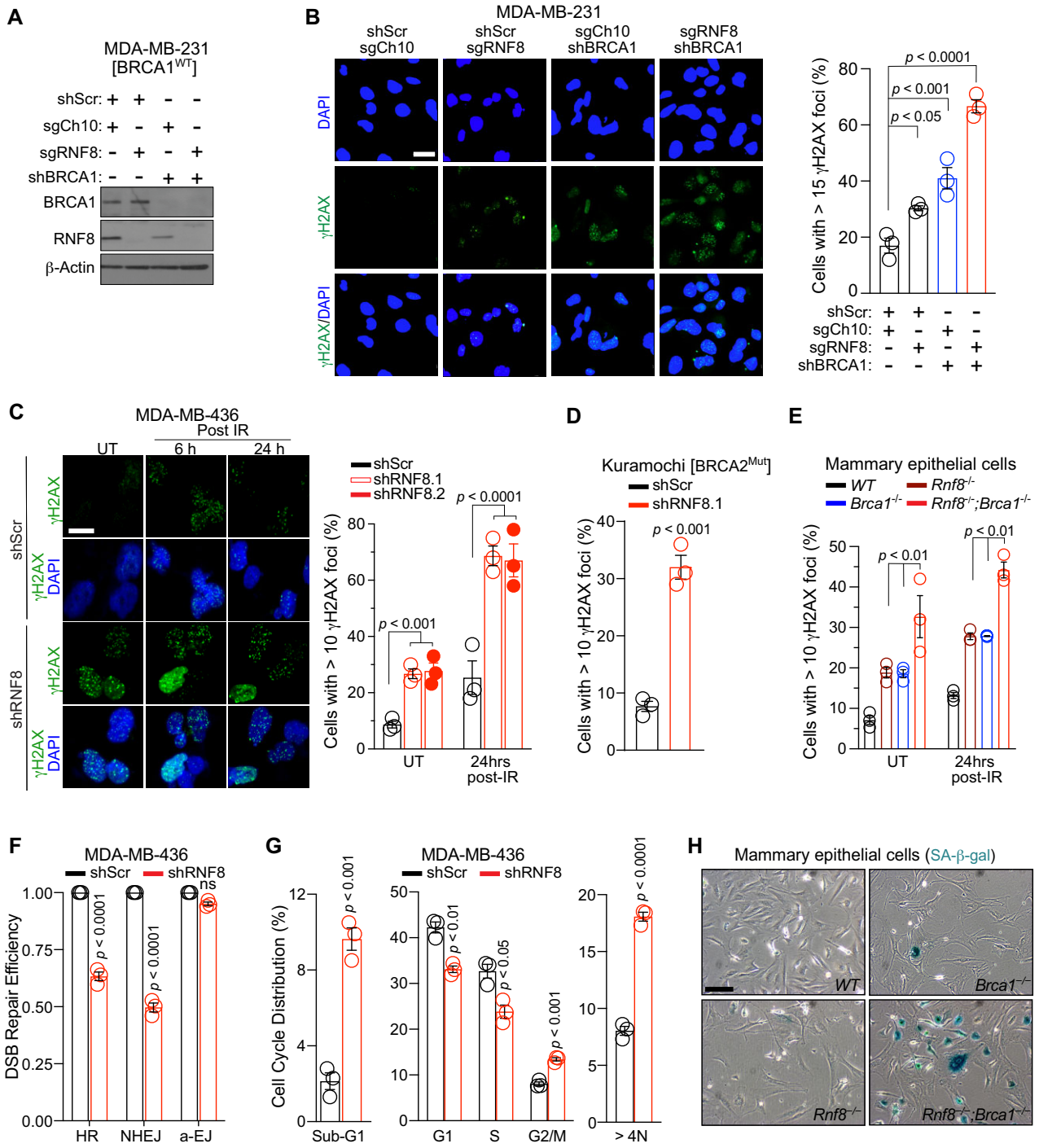

Figure 2. RNF8 depletion increases genomic instability and senescence in BRCA1/2-deficient cells. (**A**) Western blot analysis of the indicated MDA-MB-231 cells. β-Actin was used as a loading control. (**B**) The indicated MDA-MB-231 cells were stained with anti-γH2AX and DAPI, and cells with more than 15 γH2AX foci were quantified. Scale bar, 25 μm; $n = 3$. (**C**) The indicated MDA-MB-436 cells (untreated (UT), 6 or 24 h post-IR 8Gy) were stained with anti-γH2AX and DAPI, and cells with more than 10 γH2AX foci were scored. Scale bar, 25 μm; $n = 3$. (**D**) The indicated Kuramochi cells were stained with anti-γH2AX, and cells with more than 10 γH2AX foci were scored. Scale bar, 25 μm; $n = 3$. (**E**) Quantification of γH2AX staining of the indicated Mammary epithelial cells ($n = 3$). (**F**) Box plots depicting the efficiency of DSB repair pathways (homologous recombination (HR), non-homologous DNA end joining (NHEJ), and alternative end-joining (a-EJ) pathways) in mediating the repair of I-SceI–induced DSBs in indicated cells ($n = 3$). (**G**) Cell cycle distribution analysis using live Hoechst staining of the indicated cells ($n = 3$). (**H**) Representative images of SA-β-gal staining of the indicated mammary epithelial cells. Scale bar, 100 μm; $n = 3$. Graphs are depicted as mean ± SEM unless otherwise indicated. Data were analyzed using a one-way ANOVA with Tukey's multiple comparisons test (B, C, E), unpaired Student's *t* test (D, G) and unpaired *t*-test with Welch's correction (F). ns: not significant. WT: wildtype. Mut: mutant.

damage at transcription termination pause sites (42). Based on this, we sought to determine the effect of RNF8 loss on R-loop formation in *BRCA1*-mutant cancer cells. Initially we utilized S9.6 immunofluorescence, which can recognize DNA–RNA hybrids. Importantly, to ensure that the S9.6 antibody was not detecting single- and double-strand RNA, all coverslips were subjected to RNaseT1 and RNaseIII treatment prior to immunofluorescence. This analysis revealed a marked increase in nucleoplasmic (Nuclear minus nucleolar) and nucleolar R-loop levels in shRNF8 MDA-MB-436 cells compared to RNF8-proficient controls (Supplementary Figure S6b). To corroborate these observations, genomic DNAs was isolated from RNF8-deficient and -proficient MDA-MB-436 cells and subjected to dot blot analysis using S9.6 antibody. Pretreatment of the genomic DNA with RNaseH was used to validate the specificity of S9.6 antibody. Consistent with the S9.6 immunofluorescence data, the dot blot assay indicated increased S9.6 intensity in RNF8 deficient MDA-MB-436 cells compared to controls (Supplementary Figure S6c). To further strengthen these findings, we used purified catalytically inactive GFP-tagged recombinant RNaseH1 (GFP-dRNH1) as an alternative tool to visualize R-loops using fluorescence microscopy (43,44). Again, we found that depletion of RNF8 in MDA-MB-436 cells resulted in a significant increase in R-loops as judged by the nuclear GFP-dRNH1 signal (Figure 3A and B).

Next, using DNA–RNA immunoprecipitation sequencing (DRIP-seq) we examined the global distribution of R-loops in RNF8 depleted MDA-MB-436 cells and their shScr controls. Results from the DRIP-seq identified a significant increase in S9.6 enrichment in RNF8-depleted MDA-MB-436 cells compared to shScr controls (Figure 3C; Supplementary Figure S6d–f). Importantly, we observed a depletion of S9.6 signal in RNaseH treated compared to untreated samples (Supplementary Figure S6d–f). Notably, DNA–RNA hybrids in RNF8-depleted cells were significantly enriched around the gene bodies of protein coding genes and at transcription termination sites (TTS), with the most significant enrichment of R-loops at TTS (Figure 3C, Supplementary Figure S6d–f). Interestingly, there was no significant difference of DRIP signal around transcription start sites (TSS; Supplementary Figure S6e). This is consistent with published data demonstrating that R-loops form at highly transcribed GC-rich sequences and regulate gene expression by associating with both promoters and terminator regions (45).

To examine the mechanisms by which RNF8 regulates R-loop levels, we first investigated whether RNF8 localizes to R-loop prone loci in MDA-MB-436 cells by chromatin immunoprecipitation (ChIP) using an antibody targeting endogenous RNF8. To analyze the binding of RNF8 to R-loop prone loci, we performed ChIP experiments using three R-loop positive loci (AFAP1, ZNF425 and HNRNPUL2) and two R-loop negative loci (PRKCSH and TAF4) identified from the DRIP-seq data. ChIP-qPCR experiments showed a significant enrichment of RNF8 at the R-loop positive loci and no significant RNF8 binding was observed at the R-loop negative loci (Figure 3D). Additionally, we analyzed the RNF8 recruitment to the actively transcribed genes which are known to be R-loop prone loci (42,46). We observed a significant enrichment at the 5′ promoter, 5′ pause, pause regions of the *β-ACTIN* (*ACTB*) gene and endosulfine alpha (*ENSA*) gene pause site (Supplementary Figure S6g).

To further validate the DRIP-Seq data and to examine the correlation between low RNF8 expression and R-loop accumulation in BRCA1-deficient cells, we performed DRIP assays utilizing the S9.6 antibody. We examined DNA–RNA hybrid enrichments at several R-loop prone loci, including the ribosomal DNA (rDNA) repeats, telomeric repeats, *ENSA* gene transcriptional pause site, and multiple locations along the *ACTB* gene in Dox-inducible shRNF8 and shScr MDA-MB-436 cells. Depletion of RNF8 in BRCA1-deficient MDA-MB-436 and MDA-MB-231cells significantly increased DNA–RNA hybrid levels at rDNA repeats, telomeric repeats, and the *ENSA* gene transcriptional pause site (Supplementary Figure S7a,b). Similarly, RNF8 depleted MDA-MB-436 cells showed increased DNA–RNA hybrids at the 5′ pause, pause, C, and D regions of the *ACTB* gene (Supplementary Figure S7c). Notably, the S9.6 signal was depleted following treatment with RNaseH (47) indicating that the S9.6 signal is specific to DNA–RNA hybrids (Supplementary Figure S7a-c). Consistent with the DRIP-Seq data, results from the DRIP-qPCR showed that RNF8 depletion specifically increased R-loop accumulation across the gene body and TTS in *ACTB* gene but not the promoter site (Supplementary Figure S7c). To ensure the specificity of pull down using S9.6 antibody, we analyzed the levels of DNA–RNA hybrids at three R-loop positive loci (AFAP1, ZNF425 and HNRNPUL2) and two R-loop negative loci (PRKCSH and TAF4) from the DRIP-seq data. DRIP-qPCR confirmed the enrichment of R-loops at the positive loci and no significant change was observed at the negative loci (Supplementary Figure S7d). Together, our data generated using GFP-dRNH1 and S9.6 immunofluorescence, R-loop dot blot assay, DRIP-Seq and DRIP-qPCR reveal that loss of RNF8 increases R-loop levels in BRCA1-proficient breast cancer cells, and that dual loss of RNF8 and BRCA1 further exacerbates the accumulation of R-loop structures at multiple genomic loci.

Given the elevated DNA damage in *BRCA1*-mutant cells depleted of RNF8 and the role of excessive R-loops in compromising genomic integrity (9), we sought to examine whether a correlation existed between R-loop accumulation in these cells and the elevated levels of DNA damage. First, we performed ChIP-qPCR using the γH2AX antibody and observed an increased enrichment of γH2AX at specific regions of the *ACTB* gene, rDNA repeats and the *ENSA* transcriptional pause-site in RNF8-depleted MDA-MB-436 cells compared to their shScr controls (Supplementary Figure S7e). Furthermore, ectopic expression of RNaseH in RNF8-depleted MDA-MB-436 cells was found to significantly reduce the levels of DNA damage (Figure 3e). These data suggest that R-loop accumulation may be causing the increased genomic instability we observed with loss of RNF8 in *BRCA1*-mutant cells.

RNF168 cooperates with RNF8 to mediate DSB signaling and repair (11–13). RNF8-mediated histone H1 ubiquitylation facilitates RNF168 recruitment to DSBs and promotes ubiquitylation cascade to recruit various

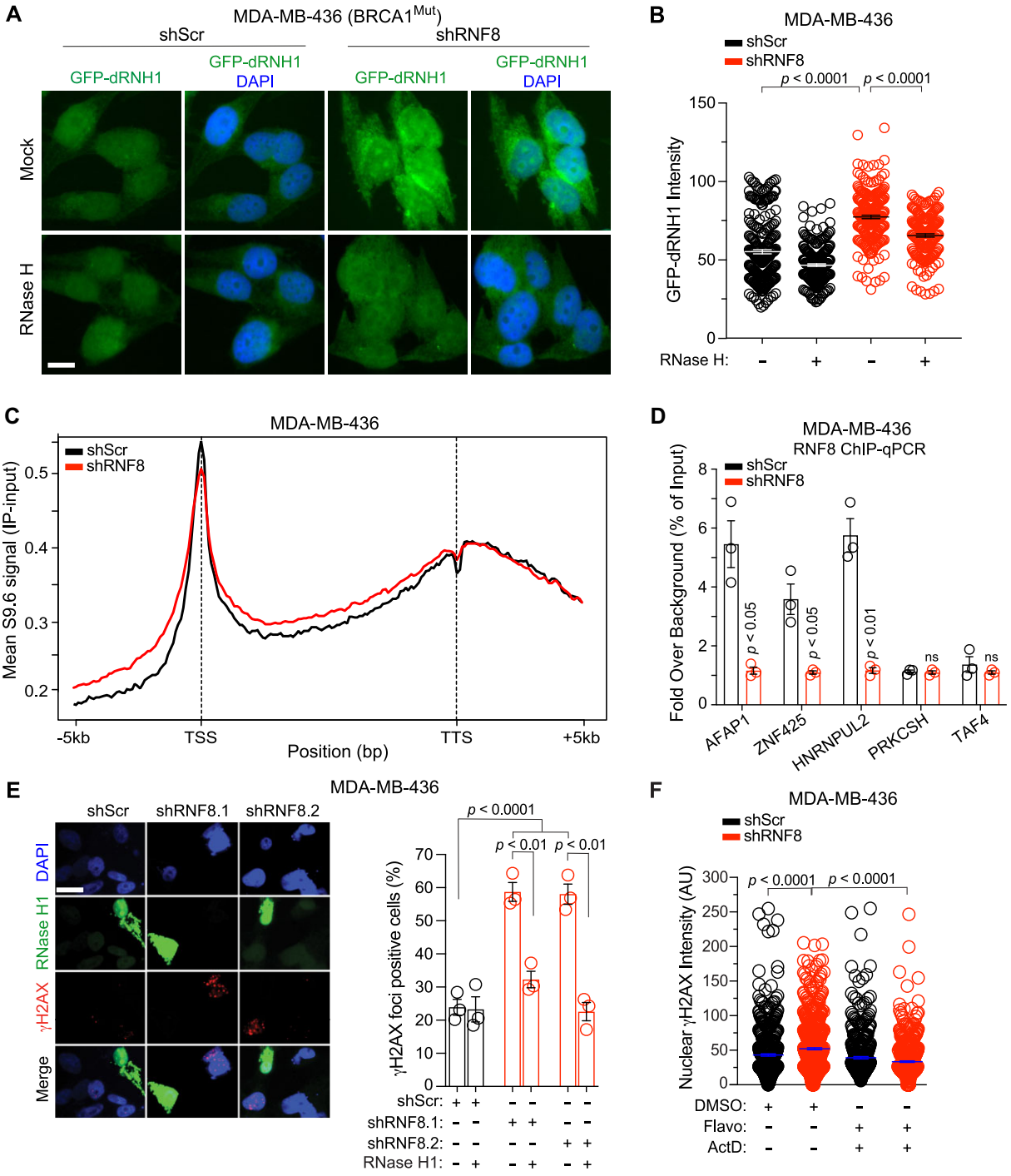

Figure 3. RNF8 deficiency in *BRCA1* mutant breast cancer cells potentiates R-loop accumulation leading to increased genomic instability. (**A, B**) Representative images and quantification of R-loop levels as detected by GFP-tagged dRHN1 in indicated cells after mock or RNaseH treatment. Bar = 25 μm. (**C**) Metagene plot of the distribution of S9.6 signals (IP-Input) along all the expressed protein coding genes (TPM > 0; 12 080 genes) and flanking regions (±5 kb) in control (blue) and shRNF8 (purple) MDA-MB-436 cells. (**D**) ChIP-qPCR analysis of RNF8 recruitment to the R-loop positive (AFAP1, ZNF425 and HNRNPUL2) and R-loop negative (PRKCSH and TAF4) loci ($n = 3$). (**E**) Representative images of RNaseH1 and γH2AX staining of the indicated MDA-MB-436 cells transiently transfected with RNaseH1. Scale bar, 10 μm. γH2AX foci were counted only in RNaseH1 overexpressing cells ($n = 3$). More than 200 nuclei were scored per condition. (**F**) Quantification of nuclear γH2AX foci in the indicated cells post-treatment with flavopiridol (Flavo) and actinomycin D (ActD) or vehicle control ($n = 3$). Scale bar = 25 μm; $n = 3$. Graphs are depicted as mean ± SEM. Data were analyzed using a Mann–Whitney *U* test (B, F), a two-tailed unpaired student's *t*-test (D), and a one-way ANOVA with Tukey's multiple comparisons test (E). Mut: mutant.

repair factors to these DNA damage sites (12). Given that RNF168 interacts with the R-loop-resolving helicase DHX9 to suppress excessive R-loop formation (48), we investigated whether the RNF8 mediated resolution of R-loops was dependent on RNF168. Interestingly, in contrast with RNF168, we failed to detect RNF8 interaction with DHX9 using co-immunoprecipitation (Supplementary Figure S7f). Furthermore, RNF168 ChIP-qPCR using RNF8-deficient and -proficient MDA-MB-436 cells showed that RNF8 deficiency had no significant effect on RNF168 recruitment to R-loop prone sites (Supplementary Figure S7g). Collectively, these data suggest that RNF8 mediates R-loop resolution independently of RNF168.

Given our observation that EU staining is increased in cells lacking both RNF8 and BRCA1, suggestive of their aberrant transcription (Supplementary Figure S6a), we evaluated whether transcription-induced DNA damage underpinned the increased genomic instability in RNF8-depleted BRCA1-proficient and deficient cells. To this end, RNA synthesis was transiently inhibited in RNF8-depleted MDA-MB-436 and MDA-MB-231 cells using the transcription inhibitors flavopiridol and actinomycin D (ActD) and then stained for γH2AX as a marker of DNA damage. We observed a significant decrease in γH2AX nuclear intensity in RNF8-deficient MDA-MB-436 and MDA-MB-231 cells treated with these transcription inhibitors compared to untreated cells (Figure 3F and Supplementary Figure S8a–d), indicating that transcriptional dysregulation in RNF8 depleted BRCA1-proficient and deficient cells may contribute to the elevated level of genomic instability. Of note, we observed higher levels of DNA damage in RNF8 depleted MDA-MB-231 cells (Figure 2B), indicating that the aberrant transcription upon RNF8 depletion is not dependent on BRCA1.

Since we observed a significant change in γH2AX nuclear intensity in RNF8-deficient MDA-MB-436 cells upon treatment with low concentration of ActD, which inhibits RNAPI-dependent rDNA transcription (49), we examined the presence of γH2AX in regions positive for the nucleolar marker nucleolin. Our data revealed that a subset of γH2AX foci in RNF8-deficient MDA-MB-436 cells were colocalizing with nucleolin (Supplementary Figure S8e, f). Collectively, our data reveal RNF8 enrichment at R-loop prone loci and that its loss promotes R-loop accumulation, leading to elevated genomic instability in *BRCA1*-mutant cancer cells.

RNF8 loss triggers replication stress in *BRCA1*-mutant breast cancer cells

The inability of cells to resolve replication stress can lead to genomic instability and cancer (50). R-loop accumulation introduces obstacles to replication forks, forcing them to stall, thereby resulting in TRCs (9,51–53). Given that RNF8 depletion in *BRCA1*-mutant cells resulted in increased R-loop accumulation and transcription-dependent DNA damage, we hypothesized that TRCs might be significantly higher in the absence of RNF8. To examine TRCs in shRNF8 and shScr MBA-MD-436 cells, we performed a proximity ligation assay (PLA) using antibodies against RNA polymerase II (RNAP II; a marker for transcription) and proliferating cell nuclear antigen (PCNA; a marker for replication). Notably, we found a significant increase in RNAP II-PCNA PLA foci in RNF8-depleted MDA-MB-436 cells compared with shScr controls, indicative of more TRCs arising as a consequence of loss of RNF8 and BRCA1 (Figure 4A). Since loss of BRCA1 compromises replication fork stability and increases replication stress (41), we used the DNA fibre assay (54) to investigate the effect of RNF8-deficiency on replication fork progression in MBA-MD-436 cells. In keeping with more TRCs, we observed that loss of RNF8 in MDA-MB-436 cells caused a significant decrease in the percentage of ongoing forks and an increase in the amount of replication fork stalling (Figure 4B–D). Consistent with the elevated levels of fork stalling, we found an increase in the asymmetry of bidirectional replication forks in shRNF8 MDA-MB-436 cells relative to the shScr controls (Figure 4E). Together, these data indicate the increased DNA replication stress in *BRCA1*-mutated cells depleted of RNF8 may arise due to elevated levels of TRCs.

Several factors are essential to mediate the cellular response to replication stress (9). For instance, replication fork stalling triggers phosphorylation and activation of the kinase ATR. This event results in the phosphorylation of other factors such as replication protein A (RPA32) and the subsequent activation of the replication stress response pathway. Therefore, we examined the effect of RNF8 knockdown on the activation of the replication stress pathway in MDA-MB-436 cells. Depletion of RNF8 in the MDA-MB-436 cells moderately raised the level of pATR-Ser428 and pRPA32-Ser33 without changing the expression of total ATR and RPA32, indicating that the increased replication stress in cells lacking both RNF8 and BRCA1 is sufficient to trigger activation of the ATR-dependent DNA damage response (Figure 4F).

To validate the role of aberrant transcription and replication in TRCs, we measured the levels of RNAP II-PCNA PLA foci in RNF8-depleted MDA-MB-436 cells upon inhibition of transcription and replication using ActD and aphidicolin (APH) (Figure 4G) respectively. These analyses indicated that the elevated level of TRCs in RNF8-depleted MDA-MB-436 cells is significantly decreased following transient inhibition of transcription or replication. TRCs constitute a major intrinsic source of genomic instability (8,9,52,53). Therefore, we measured the levels of DNA damage in RNF8-depleted cells upon transcription and replication inhibition using ActD and APH, respectively. We observed a significant decrease in γH2AX nuclear intensity in RNF8-deficient MDA-MB-436 cells treated with these inhibitors compared to untreated cells (Figure 4H). These results indicate that TRCs represent a potent source of genomic instability in these cells. Together, these findings suggest that RNF8 deficiency in *BRCA1*-mutant cells induces aberrant transcription, leading to replication stress, TRCs and further impairment of genomic integrity.

RNF8 interacts with XRN2, promoting its ubiquitylation and enrichment at R-loop-prone loci

To gain insight into the molecular mechanisms that drive the accumulation of R-loops in the absence of RNF8, we searched for RNF8 interactors by coupling mass

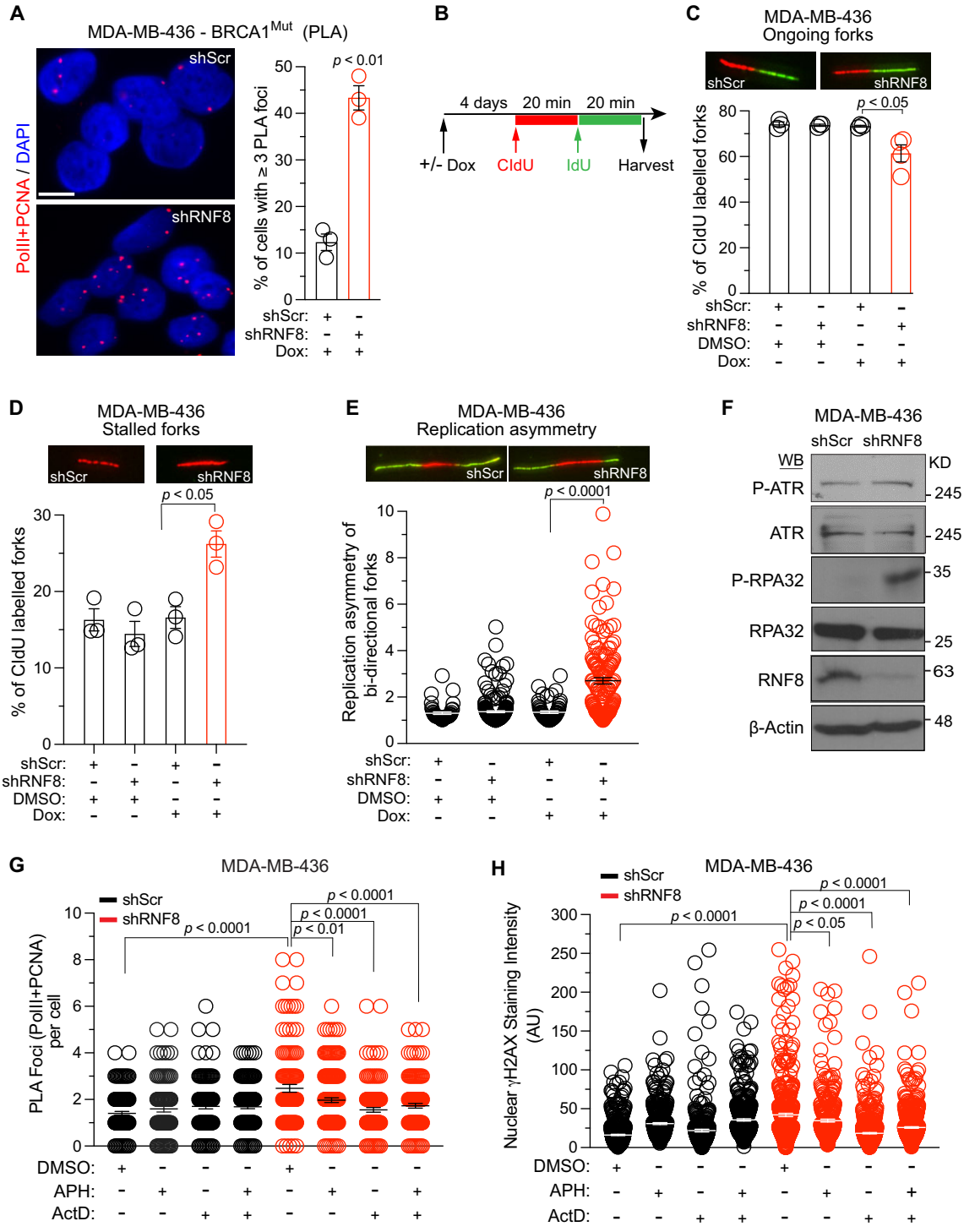

Figure 4. RNF8 deficiency promotes replication stress in *BRCA1*-mutant breast cancer cells. (**A**) Representative images and quantification of PLA foci indicating the interaction between RNA Pol II and PCNA (scale bar = 25 μm; $n = 3$). (**B**) Schematic of the experimental design used for DNA fibre analysis. shRNF8 and shScr MDA-MB-436 cells were treated with Dox for 4 days and sequentially pulse-labelled with two thymidine analogues CldU and IdU for 20 min each before being harvested for DNA fibre analysis. (**C. D**) The percent of ongoing and stalled replication forks in the indicated cells is plotted and representative images are shown. (**E**) The replication fork asymmetry in the indicated cells is plotted and representative images are shown. For the replication fork structures (C. D: ongoing and stalled forks) more than 1250 CldU-labelled fibres in total were counted for the whole experiment. For the replication fork asymmetry (**E**) over 50 bi-directional first label origins in total were counted for the whole experiment. All the fibre data (C–E) are representative of three independent experimental replicates. (**F**) Western blot showing the expression of the indicated proteins in RNF8-depleted MDA-MB-436 cells and their shScr controls. (**G**) Quantification of PCNA-RNAPII CTD PLA foci per nucleus in the indicated MDA-MB-436 cells treated for 1hr with DMSO, APH (500 nM) or ActD (0.5 μM). (**H**) Quantification of nuclear γH2AX foci in shRNF8 and shScr MDA-MB-436 cells after 1 h treatment with APH, ActD, and DMSO as indicated ($n = 3$). Graphs are depicted as mean ± SEM. Data were analysed using two-tailed unpaired Student's *t*-test (A, C, D), Mann–Whitney *U* test (E), and one-way ANOVA with Tukey's multiple comparisons test (G, H). Mut: mutant.

spectrometry (MS) to Flag-RNF8 and Flag empty vector (Flag-EV) co-immunoprecipitation in HEK293FT cells (ftp://MSV000089537@massive.ucsd.edu). Comparing with the R-loop interactome from published studies (55,56), we analyzed the R-loop factors which were identified as RNF8 interactors from our mass spec data (Supplementary Figure S9). This analysis revealed putative interactors of RNF8 involved in different cellular processes, including RNA processing, translation, and RNA binding. One of the top hits in the RNF8-IP/MS data was XRN2, a 5′-3′ exoribonuclease 2, known to regulate transcription termination and R-loop resolution. XRN2 deficient cells display elevated levels of replicative stress and increased R-loop accumulation. Interestingly, DRIP-seq analysis of R-loop accumulation in XRN2-depleted U2OS cells identified the highest accumulation of R-loops at TTS, similar to RNF8 depleted cells (57). Based on this, we hypothesised that RNF8 and XRN2 functioned together to suppress R-loop formation and genome instability. We confirmed the interaction between endogenous XRN2 and RNF8 proteins in MDA-MB-436 and MDA-MB-231 cells using co-immunoprecipitation assay and this interaction was further validated using HEK 293FT cells transiently expressing Flag-tagged XRN2 (Figure 5A and Supplementary Figure S10a, b). Moreover, using domain-mapping assays, we demonstrated that XRN2 interacts with RNF8 through its 5′-3′ exonuclease N-terminal domain (Figure 5B).

Given the interaction of RNF8 with XRN2, we examined the effect of RNF8 deficiency on XRN2 expression. Our data indicated that loss of RNF8 has no effect on the expression of XRN2 protein in MDA-MB-436 and MDA-MB-231 cells (Figure 5C). Since XRN2 interacts with RNF8 and is ubiquitylated on several lysine residues (https://thebiogrid.org/116483/summary/homo-sapiens/xrn2.html), we examined whether RNF8 could mediate XRN2 ubiquitylation in *BRCA1* proficient and deficient cells. Thus, we performed ubiquitylation assays and examined XRN2 ubiquitylation in the presence or absence of RNF8. RNF8 depletion decreased the extent of XRN2-associated Ub smears in MDA-MB-436 and MDA-MB-231 cells, suggesting that XRN2 ubiquitylation is dependent on RNF8 (Figure 5D, E). In support of this, overexpression of WT RNF8 but not a catalytically dead mutant (C406S) in HEK293T cells significantly increased XRN2 ubiquitylation (Figure 5F). Next, we performed *in vitro* ubiquitylation assay and examined whether RNF8 directly ubiquitylates XRN2. We observed strong ubiquitylation of recombinant XRN2 in the presence of recombinant RNF8, E1, E2 and Ub proteins (Figure 5G). However, *in vitro* ubiquitylated XRN2 was not observed when ubiquitin was omitted from this assay. These data indicate that XRN2 is a novel and direct ubiquitylation substrate for RNF8.

Since RNF8 depletion did not affect XRN2 protein levels (Figure 5C), we hypothesised that the RNF8-dependent XRN2 ubiquitylation may regulate its binding to sites of R-loops. Interestingly, XRN2 binding to three R-loop positive loci (AFAP1, ZNF425 and HNRNPUL2) was decreased upon RNF8 depletion and no significant difference in binding was observed at R-loop negative loci (PRKCSH and TAF4) (Figure 5H). Additionally, loss of RNF8 significantly decreased the occupancy of XRN2 at the R-loop prone loci rDNA, telomeric repeats, and specific sites within the *ACTB* gene (Supplementary Figure S10c).

Given that R-loop resolution over the GC-rich pause sites by SETX allows the binding of XRN2 to promote transcription termination (46), we next investigated whether the SETX occupancy at R-loop sites is affected by RNF8 deficiency in MDA-MB-436 cells. Interestingly, SETX binding to the 5′ promoter, pause and C regions of *ACTB* gene was significantly decreased upon RNF8 depletion (Supplementary Figure S10d). Thus, defective XRN2 recruitment to R-loop-enriched loci and increased accumulation of R-loops in RNF8 depleted *BRCA1* mutant cancer cells might be partially due to a reduction in SETX recruitment to R-loops.

To understand the functional consequences of RNF8-XRN2 interaction, RNF8-depleted MDA-MB-436 cells reconstituted with RNF8-WT or RNF8-C406S mutant were examined for XRN2 recruitment to R-loop prone loci. Whilst RNF8-WT restored XRN2 recruitment to the rDNA, telomeric repeats, and specific sites within the *ACTB* gene in RNF8-depleted cells, a catalytically inactive RNF8 mutant did not (Figure 6A). While RNF8 depletion in MDA-MB-436 cells significantly increased GFP-dRNH1 nuclear staining, reconstitution of these RNF8-depleted cells with RNF8-WT significantly decreased GFP-dRNH1 nuclear staining (Supplementary Figure S10e). However, R-loop levels remained comparable in shRNF8 MDA-MB-436 cells, and their counterparts reconstituted with RNF8-C406S mutant (Supplementary Figure S10e). Next, we generated shXRN2 MDA-MB-436 cells and their shScr controls and examined the effect of XRN2 deficiency on DNA damage, R-loop accumulation, and transcription. Similar to the loss of RNF8, XRN2 deficient MDA-MB-436 cells also showed a significant increase in the level of DNA damage and nuclear GFP-dRNH1 signal (Figure 6B–D). Furthermore, we observed that depletion of XRN2 in MDA-MB-436 cells led to a significantly reduced colony-forming ability (Figure 6E). However, consistent with a previous report (58), XRN2 depletion in *BRCA1*-mutant cells did not affect transcription rate (Supplementary Figure S10f) nor the recruitment of RNF8 to R-loops prone sites in the *ACTB* gene (Supplementary Figure S10g). Taken together, we conclude that RNF8 interacts with XRN2 to mediate its ubiquitylation and recruitment at R-loop-prone loci to resolve R-loops and preserve genome stability.

DISCUSSION

BRCA1 mutations predispose for breast, ovarian and other cancers (1,2). Studies of synthetic lethal interactions revealed potential therapeutic targets for *BRCA1*-mutant cancers (2,35,36,59). The approval of PARP inhibitors to treat advanced and metastatic breast, ovarian and pancreatic cancers with *BRCA1/2* mutations illustrates how synthetic lethal interactions can be exploited for cancer therapy. However, drug resistance remains a significant limitation of PARPi, highlighting the need for novel and more effective therapies for these high-risk cancer patients (2).

In the present study, we uncovered that RNF8 is essential for the survival of human breast and ovarian cancer

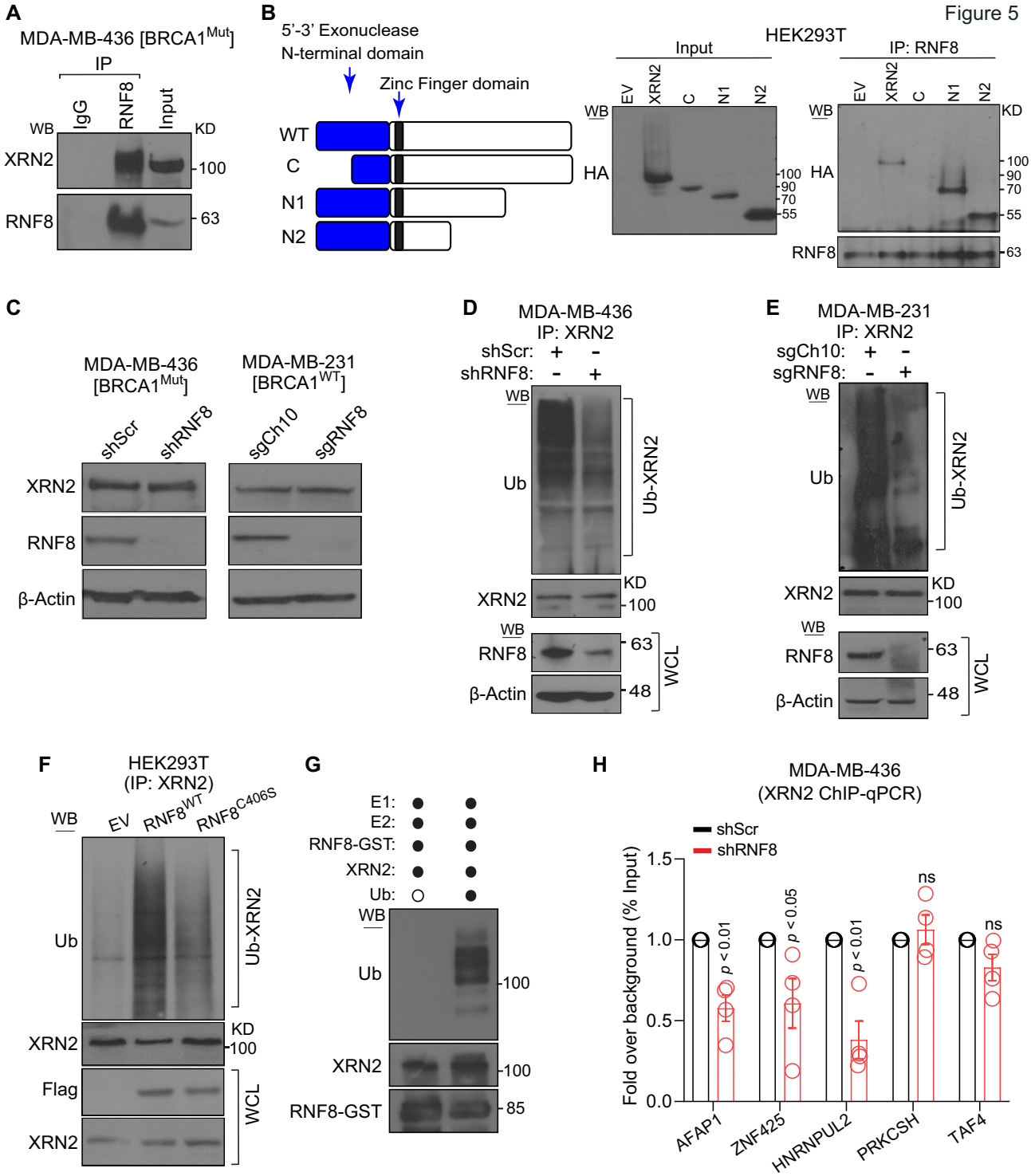

Figure 5. RNF8 interacts with XRN2, mediating its ubiquitylation and recruitment to R-loop-prone loci. (**A**) Interaction of endogenous RNF8 and XRN2 in MDA-MB-436 cells was examined by IP/WB as indicated. (**B**) Schematic of XRN2 full length wildtype (WT), its deletion mutants, and IP/WB showing XRN2 domains interacting with RNF8. (**C**) Representative WB showing the expression of XRN2 protein in the indicated MDA-MB-436 and MDA-MB-231 cells. (**D, E**) Representative WB of the indicated MDA-MB-436 and MDA-MB-231 cells subjected to IP with anti-XRN2 antibody followed by immunoblotting using anti-Ubiquitin (Ub) antibodies. WB analysis confirmed the IP of XRN2 and indicated the level of RNF8 and β-Actin in WCL. (**F**) HEK293T cells were transfected with indicated Flag-tagged mouse Rnf8, RNF8^{C406S} and empty vector (EV) as indicated. WCL were subjected to IP with anti-XRN2 antibody and membrane was probed with anti-ubiquitin antibody. In vivo ubiquitylation of XRN2 in indicated cells is shown. (**G**) *In vitro* ubiquitylation of recombinant XRN2 in the presence of recombinant RNF8, UBE1 (E1), UBE2 (E2) and Ub proteins. (**H**) ChIP-qPCR analysis of shRNF8 and shScr MD-MB-436 cells for XRN2 recruitment to R-loop positive (AFAP1, ZNF425 and HNRNPUL2) and negative (PRKCSH and TAF4) loci in indicated cells ($n = 4$). Graphs are depicted as mean ± SEM. The data was analyzed using a two-tailed unpaired Student's *t*-test (G). ns: not significant.

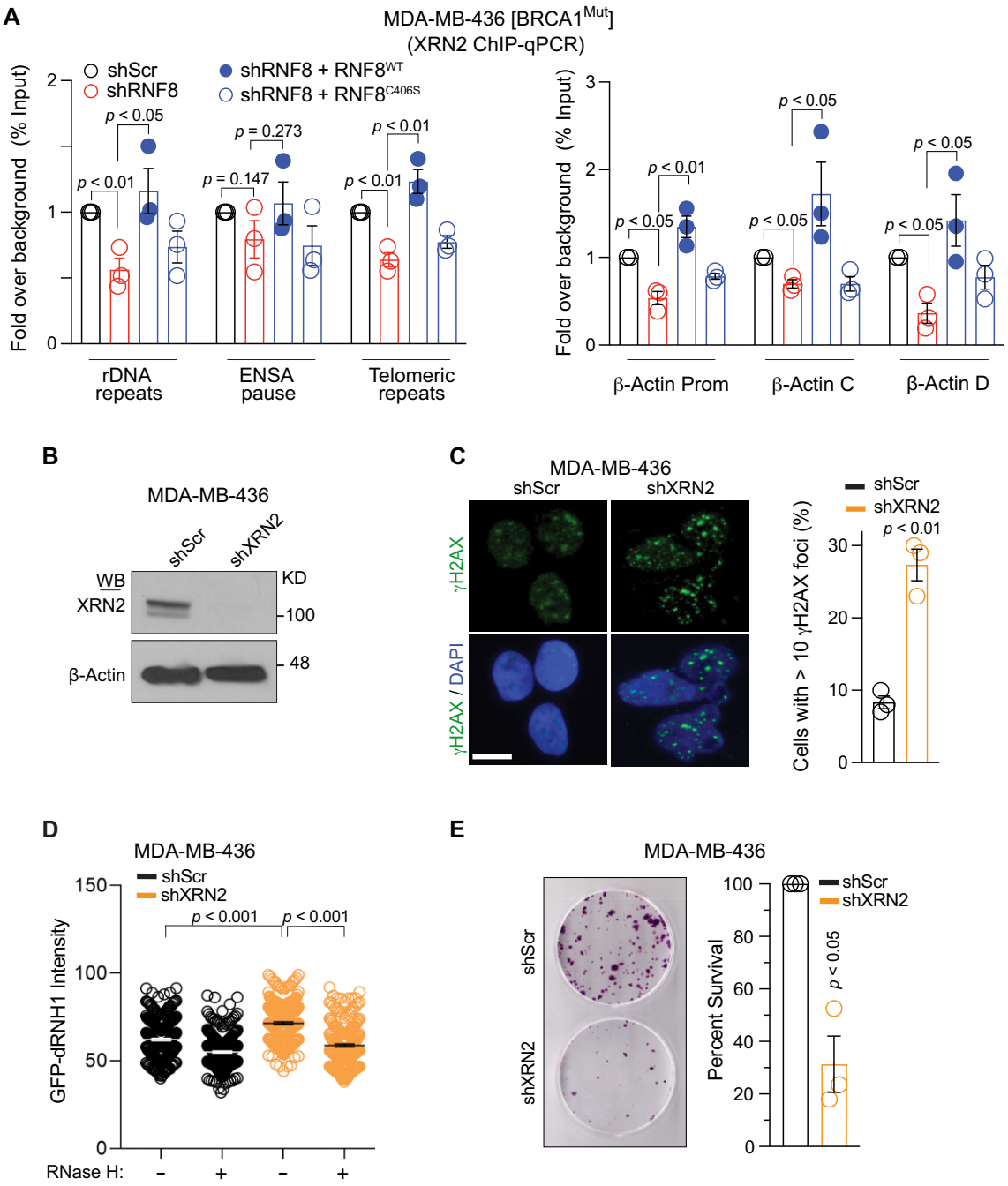

Figure 6. Reconstitution of RNF8-depleted cells with wildtype RNF8 rescues XRN2 recruitment to R-loops. (**A**) Anti-XRN2 ChIP-qPCR was performed using MDA-MB-436 cells to examine the effect of RNF8-WT and its C406S mutant on the recruitment of XRN2 to the indicated R-loop–prone loci ($n = 3$). (**B**) Representative WB validating XRN2 knockdown in MDA-MB-436 cells. (**C**) Representative images and quantification of γH2AX foci in shXRN2 and shScr MDA-MB-436 cells ($n = 3$). Scale bar, 25 μm. (**D**) Quantification of R-loop levels as detected by GFP-tagged dRHN1 in indicated cells after mock or RNaseH treatment. ($n = 3$; Bar = 25 μm). (**E**) Representative images and quantification of the colony-forming ability of shXRN2 and shScr MDA-MB-436 cells ($n = 3$). Graphs are depicted as mean ± SEM. The data was analyzed using the 2-way ANOVA with Tukey's multiple-comparison test (A), two-tailed unpaired Student's *t*-test (C), Mann–Whitney *U* test (D), unpaired *t*-test with Welch's correction (E). ns: not significant. Prom: promoter.

cell with mutations in *BRCA1* or *BRCA2*. Using a mouse model for *BRCA1*-mutant breast cancer, we demonstrated that genetic deletion of *Rnf8* in the mammary epithelial cells of *Brca1* mutant female mice remarkably reduces their risk for mammary tumorigenesis. Consistent with this finding, the TCGA breast cancer dataset analysis indicates that *RNF8* is expressed at a higher level in HR-defective tumors than those proficient in HR-mediated repair. Interestingly, among the key factors functioning in the HR pathway, the expression of the *RNF8* gene was significantly higher in HR-defective TCGA BRCA TNBC dataset.

Previous studies have demonstrated that loss of 53BP1, a factor important for NHEJ repair, restores HR and genomic stability in *BRCA1*-mutant cells (14,15). Furthermore, 53BP1 deficiency protects *Brca1*-mutant mouse models from mammary tumorigenesis (14). In contrast, our data indicate that although TNBC cells deficient for both RNF8 and BRCA1 fail to recruit 53BP1 to sites of DNA damage, these cells display a reduction rather than restoration of HR-dependent repair. As a consequence, unlike 53BP1 loss, compromising RNF8 function in breast and ovarian cancer cells lacking BRCA1 or BRCA2 exacerbated the endogenous levels of spontaneous and IR- or olaparib-induced genome instability. This indicates that although RNF8 is critical for recruiting 53BP1 to sites of DNA damage, loss of RNF8 in the context of an HR deficiency has opposing consequences to loss of 53BP1 i.e. synthetic lethality versus synthetic viability.

Excessive genomic instability promotes senescence and cell death, contributing to the suppression of tumor growth (38). Consistent with their elevated levels of DNA damage, TNBC cells and mammary epithelial cells depleted of both RNF8 and BRCA1 exhibited increased cellular senescence. Moreover, orthotopic xenografts of BRCA1-mutant TNBC cell lines further confirmed that RNF8 confers survival of BRCA1-mutant TNBC tumors *in vivo*. This finding agrees with the preventive effect of Rnf8 deficiency on the development of mammary tumors in Brca1-mutant mouse models.

Genomic instability results from impaired DNA damage repair but can also be a consequence of aberrant R-loops, increased transcription and replication, and transcription-replication collisions (8,9,51–53). In this study, we report a novel function of RNF8 in facilitating the resolution of R-loops. We demonstrated that RNF8 is enriched at R-loop-prone genomic loci, particularly TTS, and that RNF8 deficiency in BRCA1-mutant TNBC cells resulted in R-loop accumulation and DNA damage at those R-loop enriched sites. Overexpression of exogenous RNaseH in TNBC cells deficient for both RNF8 and BRCA1 significantly reduced their levels of DNA damage, suggesting that R-loop accumulation contributes to their genomic instability.

A growing number of factors, including the 5′-3′ exoribonuclease XRN2, have been identified for their important roles in the resolution of R-loops (8). XRN2 is a critical for transcription termination, degradation of RNA and the resolution of R-loop structures (60). Similar to XRN2 depleted cells (57), RNF8 depletion significantly increased R-loop accumulation at TTS, suggesting that XRN2 and RNF8 might function co-operatively to resolve R-loops. Through this study, we have identified that RNF8 directly ubiquitylates XRN2. In BRCA1-deficient cells, RNF8 ubiquitylated XRN2 to facilitate its recruitment to R-loop prone loci. This mechanism regulated excessive R-loops accumulation, which can lead to genomic instability and replication stress. Consistent with this, we observed defective XRN2 recruitment to R-loop prone loci, and increased R-loops level in RNF8 depleted BRCA1 mutant cells. Reconstitution of these RNF8 depleted BRCA1 mutant cells with $RNF8^{WT}$, but not its E3 ligase dead mutant ($RNF8^{C406S}$), rescued XRN2 binding to R-loop prone loci and restrained R-loop levels. Collectively our data indicated that RNF8 mediates XRN2 ubiquitylation to facilitate its recruitment to R-loop-enriched genomic loci and the resolution of DNA–RNA hybrids. Whilst the mechanism with which RNF8 regulates the recruitment of XRN2 to R-loops through ubiquitylation remains unclear, it is plausible that XRN2 ubiquitylation increases its affinity for DNA–RNA hybrids and/or enhances its nucleolytic activity. However, these possibilities require further investigation. Previous studies reported the importance of the helicase SETX for R-loops dissolution and transcription termination (46,61). Our examination of the effect of RNF8 loss on SETX occupancy at R-loop sites indicated a significant decrease of SETX binding to the 5′ promoter, pause and C regions of *ACTB* gene in breast cancer cells lacking both RNF8 and BRCA1. Thus, enhanced R-loops accumulation specifically at TTS in RNF8 depleted BRCA1 mutant cancer cells might be partially due to defective XRN2 and SETX recruitment to R-loop prone loci. It is tempting to speculate that the higher level of DNA damage and TRC in RNF8 depleted BRCA1 mutant cancer cells may relate to the defective transcription termination in these cells. Furthermore, our proteomics studies indicated other potential RNF8 interactors with known functions in sensing and resolving R-loops. These factors engage in different processes, including RNA binding and processing (Supplementary Figure 9). Therefore, in addition to XRN2 and SETX, RNF8 might also regulate other factors involved in R-loop resolution.

Transcription promotes the formation of R-loops (62). Notably, we showed that aberrant transcription in RNF8 and BRCA1-deficient cells resulted in elevated DNA damage and replication stress. Prior studies indicated that depletion of RNF8 and RNF168 partially reversed ATM-mediated transcriptional silencing at DSB sites (39). It is therefore plausible that depletion of RNF8 in *BRCA1*-mutant cells may contribute to the reversal of transcriptional silencing, resulting in aberrant transcription. The elevated level of DNA damage upon RNF8 knockdown in *BRCA1*-mutant TNBC cells is transcription dependent as it was reversed in response to treatment with the transcription inhibitors Flavopiridol and actinomycin D. This suggests that aberrant transcription in the absence of RNF8 and BRCA1 promotes the accumulation of R-loops and increases genomic instability.

RNF8 is essential for the recruitment of RNF168 to DSB-flanking sites (63). We have recently reported that RNF168 plays a critical role in R-loop resolution by recruiting the helicase DHX9 to these hybrid structures (48). However, our data indicated that knockdown of RNF8 had no significant effect on RNF168 occupancy at R-loop-prone loci. In addition, contrasting with RNF168, RNF8 does

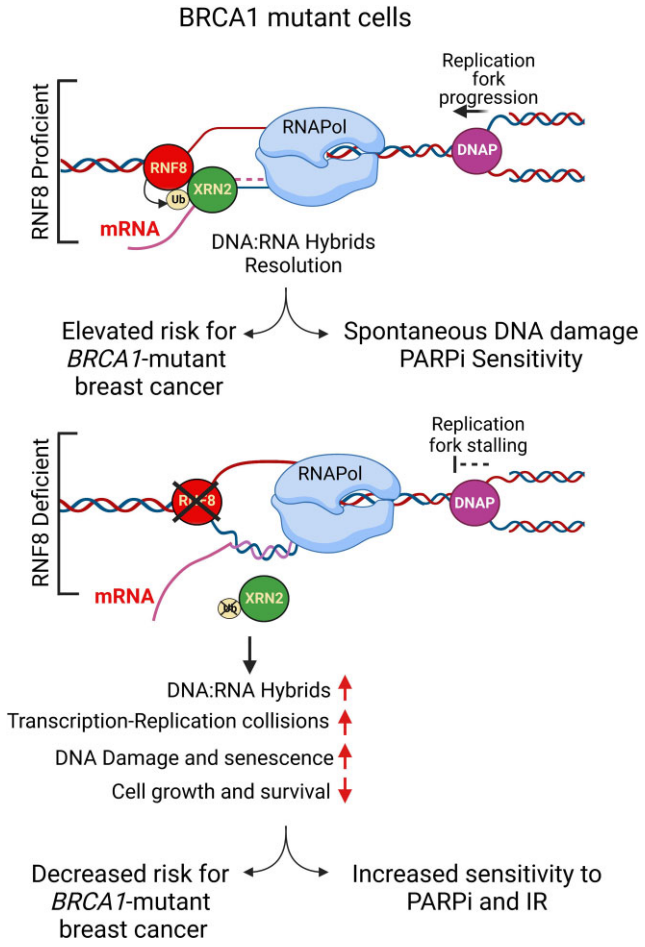

Figure 7. Schematic of RNF8 and XRN2 mediated R-loop regulation to control BRCA1-mutant cancers. The proposed model depicts a new role for RNF8 in mediating the ubiquitylation of XRN2, facilitating its recruitment to DNA–RNA hybrids. In *BRCA1* mutant cancer cells, RNF8-dependent recruitment of XRN2 to R-loops allows it to resolve the DNA–RNA hybrids, limiting genomic instability. RNF8 deficiency in *BRCA1*-mutant breast cancer cells induces R-loop accumulation and transcription-replication collisions, leading to increased DNA damage, further exacerbating genomic instability, senescence, and growth defects in these cancer cells. RNF8 deficiency also increases the sensitivity to PARP inhibitors (PARPi) and irradiation of *BRCA1*-mutant cells and protects against *BRCA1*-mutated breast cancer.

not interact with DHX9. Collectively, these data suggests that RNF8 prevents R-loops accumulation in RNF168-independent manner.

Accumulation of R-loop leads to severe replication fork slowing and DNA breakage (9). In this study, we observed that RNF8 deficiency in *BRCA1*-mutant cancer cells resulted in increased stalling and asymmetry of replication forks. Supporting a role for the aberrant R-loop accumulation in promoting replication stress and genomic instability in RNF8 depleted *BRCA1* mutant TNBC cells, treatment of these cells with the replication inhibitors aphidicolin and actinomycin D significantly reduced their levels of DNA damage.

Transcription-replication collisions are arguably the primary source of R-loop-induced DNA damage and genomic instability (8,9,51–53). In addition to R-loop accumulation and the aberrant transcription and replication in cells deficient for both RNF8 and BRCA1, our data indicated that dual loss of RNF8 and BRCA1 promotes transcription-replication collisions. Notably, TNBC cells deficient for RNF8 and BRCA1 treated with inhibitors of transcription or replication displayed reduced Transcription-replication collisions, and as a consequence restrained their level of DNA damage. These observations highlight the contribution of transcription-replication collisions to the elevated genomic instability in cancer cells deficient for both RNF8 and BRCA1. These data also indicated that RNF8 depletion in BRCA1-mutant TNBC cells deregulates several vital cellular processes, thus leading to increased transcription-replication collisions and defective growth of TNBC cells. Collectively, our data support an essential role for RNF8 in restraining breast cancer risk associated with *BRCA1* mutations. We provide evidence to support RNF8 involvement in suppressing DNA damage associated with transcription, R-loops, replication, and transcription-replication collisions in *BRCA1*-mutant breast tumors (Figure 7). These findings, together with the preventive effect of Rnf8 deficiency on mammary tumorigenesis in *Brca1*-mutant mouse models, indicate that future evaluation of RNF8 as a potential therapeutic target for cancers associated with *BRCA1* mutations is warranted.

DATA AVAILABILITY

The data underlying this article are available in GEO at https://www.ncbi.nlm.nih.gov/geo/, and can be accessed with accession number GSE202723.

ETHICS APPROVAL AND CONSENT TO PARTICIPATE

All procedures and studies involving mice were performed per the Princess Margaret Cancer Centre Animal Care Committee guidelines (Protocol numbers: 1223, 4805 and 2287).

CONSENT FOR PUBLICATION

All authors reviewed and approved this manuscript.

SUPPLEMENTARY DATA

Supplementary Data are available at NAR Online.

ACKNOWLEDGEMENTS

We thank the members of the Hakem lab for helpful discussions and Dr J. Manley and Dr K.A Cimprich for kindly sharing reagents. We also thank T. Henderson and C. Fozil for help with experiments. R.H holds the Lee K. and Margaret Lau Chair in Breast Cancer Research, a joint project between the University of Toronto and The Princess Margaret hospital, Toronto, Canada.
Authors' contributions: R.K., M.L., B.G., S.E.G., P.S.P., K.C.J.N., T.Y., K.K.N.G., J.S-G., F.M., A.S., A.A., R.E., J.M., N.K., A.P., J.H., B.H., J.J.R., M.P.H, D.S, A.S. and A.H. performed experiments, analyzed the data and prepared figures. The manuscript was written by R.K., M.L.

A.H and RH. G.W.B. supervised B.H. M.A.-J. supervised A.S. K.M., supervised T.Y., and N.K. B.R supervised J.S.-G., and A.P. M.A.P. supervised F.M. G.S.S supervised J.J.R. A.H. and R.H supervised R.K., M.L., B.G., S.E.G., P.S.P., K.C.J.N., K.K.N.G., A.A., R.E. and J.M. C.A. supervised S.D. and A.S. A.H and R.H. conceived, designed and oversaw the study.

FUNDING

Canadian Institute of Health Research [FDN-143214 to R.H., FDN-159913 to G.W.B., FDN-388879 to J.Y.M., CIHR-399687 to K.M., MOP119289 to B.R.]; Canadian Cancer Society [705367, 706439 to R.H.]; Worldwide Cancer Research [110215 to R.H.]; Carlos III Institute of Health [PI18/01029 to M.A.P.]; Generalitat de Catalunya SGR [2017-449 to M.A.P.]; CERCA Program (to M.A.P.); Quebec Breast Cancer Foundation (to M.A-J.); Cancer Research UK programme [C17183/A23303 to G.S.S.]; R.K. is supported by the Princess Margaret Cancer Foundation, the Hold'Em for Life Foundation, and the Strategic Training in Transdisciplinary Radiation Science for the 21st Century (STARS21); J.H. is supported by the Princess Margaret Cancer Foundation and CIHR fellowship; J.J.R. is supported by the University of Birmingham; Canada Graduate Scholarships, Ontario Graduate Scholarship (to M.L., A.A. and P.S.P.); STARS21, Terry Fox Foundation, Princess Margaret Cancer Foundation (to P.S.P.); B.H. was supported by an Alexander Graham Bell Canada Graduate Scholarship from the Natural Sciences and Engineering Research Council of Canada; C.H. is supported by the Structural Genomics Consortium; S.G.S. is a registered charity [1097737] that receives funds from Bayer AG, Boehringer Ingelheim, Bristol Myers Squibb, Genentech, Genome Canada through Ontario Genomics Institute [OGI-196]; EU/EFPIA/OICR/McGill/KTH/Diamond Innovative Medicines Initiative 2 Joint Undertaking [EU-bOPEN grant 875510]; Janssen, Merck KGaA (aka EMD in Canada and US), Pfizer and Takeda. Funding for open access charge: CIHR.

Conflict of interest statement. M.A.P. is the recipient of an unrestricted research grant from Roche Pharma for the support of the ProCURE study.

REFERENCES

1. Kuchenbaecker,K.B., Hopper,J.L., Barnes,D.R., Phillips,K.A., Mooij,T.M., Roos-Blom,M.J., Jervis,S., van Leeuwen,F.E., Milne,R.L., Andrieu,N. *et al.* (2017) Risks of breast, ovarian, and contralateral breast cancer for BRCA1 and BRCA2 mutation carriers. *JAMA*, **317**, 2402–2416.
2. Ashworth,A. and Lord,C.J. (2018) Synthetic lethal therapies for cancer: what's next after PARP inhibitors?*Nat. Rev. Clin. Oncol.*, **15**, 564–576.
3. Chen,C.C., Feng,W., Lim,P.X., Kass,E.M. and Jasin,M. (2018) Homology-directed repair and the role of BRCA1, BRCA2, and related proteins in genome integrity and cancer. *Annu Rev Cancer Biol*, **2**, 313–336.
4. Krais,J.J. and Johnson,N. (2020) BRCA1 Mutations in cancer: coordinating deficiencies in homologous recombination with tumorigenesis. *Cancer Res.*, **80**, 4601–4609.
5. Hill,S.J., Rolland,T., Adelmant,G., Xia,X., Owen,M.S., Dricot,A., Zack,T.I., Sahni,N., Jacob,Y., Hao,T. *et al.* (2014) Systematic screening reveals a role for BRCA1 in the response to transcription-associated DNA damage. *Genes Dev.*, **28**, 1957–1975.
6. Tarsounas,M. and Sung,P. (2020) The antitumorigenic roles of BRCA1-BARD1 in DNA repair and replication. *Nat. Rev. Mol. Cell Biol.*, **21**, 284–299.
7. Schlacher,K., Wu,H. and Jasin,M. (2012) A distinct replication fork protection pathway connects Fanconi anemia tumor suppressors to RAD51-BRCA1/2. *Cancer Cell*, **22**, 106–116.
8. Garcia-Muse,T. and Aguilera,A. (2019) R Loops: From physiological to pathological roles. *Cell*, **179**, 604–618.
9. Brickner,J.R., Garzon,J.L. and Cimprich,K.A. (2022) Walking a tightrope: the complex balancing act of R-loops in genome stability. *Mol. Cell*, **82**, 2267–2297.
10. Skourti-Stathaki,K. and Proudfoot,N.J. (2014) A double-edged sword: r loops as threats to genome integrity and powerful regulators of gene expression. *Genes Dev.*, **28**, 1384–1396.
11. Schwertman,P., Bekker-Jensen,S. and Mailand,N. (2016) Regulation of DNA double-strand break repair by ubiquitin and ubiquitin-like modifiers. *Nat. Rev. Mol. Cell Biol.*, **17**, 379–394.
12. Thorslund,T., Ripplinger,A., Hoffmann,S., Wild,T., Uckelmann,M., Villumsen,B., Narita,T., Sixma,T.K., Choudhary,C., Bekker-Jensen,S. *et al.* (2015) Histone H1 couples initiation and amplification of ubiquitin signalling after DNA damage. *Nature*, **527**, 389–393.
13. Mattiroli,F. and Penengo,L. (2021) Histone ubiquitination: an integrative signaling platform in genome stability. *Trends Genet.*, **37**, 566–581.
14. Bunting,S.F., Callen,E., Wong,N., Chen,H.T., Polato,F., Gunn,A., Bothmer,A., Feldhahn,N., Fernandez-Capetillo,O., Cao,L. *et al.* (2010) 53BP1 inhibits homologous recombination in Brca1-deficient cells by blocking resection of DNA breaks. *Cell*, **141**, 243–254.
15. Bouwman,P., Aly,A., Escandell,J.M., Pieterse,M., Bartkova,J., van der Gulden,H., Hiddingh,S., Thanasoula,M., Kulkarni,A., Yang,Q. *et al.* (2010) 53BP1 loss rescues BRCA1 deficiency and is associated with triple-negative and BRCA-mutated breast cancers. *Nat. Struct. Mol. Biol.*, **17**, 688–695.
16. Rosenthal,R., McGranahan,N., Herrero,J., Taylor,B.S. and Swanton,C. (2016) DeconstructSigs: delineating mutational processes in single tumors distinguishes DNA repair deficiencies and patterns of carcinoma evolution. *Genome Biol.*, **17**, 31.
17. Li,L., Halaby,M.J., Hakem,A., Cardoso,R., El Ghamrasni,S., Harding,S., Chan,N., Bristow,R., Sanchez,O., Durocher,D. *et al.* (2010) Rnf8 deficiency impairs class switch recombination, spermatogenesis, and genomic integrity and predisposes for cancer. *J. Exp. Med.*, **207**, 983–997.
18. McPherson,J.P., Lemmers,B., Hirao,A., Hakem,A., Abraham,J., Migon,E., Matysiak-Zablocki,E., Tamblyn,L., Sanchez-Sweatman,O., Khokha,R. *et al.* (2004) Collaboration of Brca1 and Chk2 in tumorigenesis. *Genes Dev.*, **18**, 1144–1153.
19. Elstrodt,F., Hollestelle,A., Nagel,J.H., Gorin,M., Wasielewski,M., van den Ouweland,A., Merajver,S.D., Ethier,S.P. and Schutte,M. (2006) BRCA1 mutation analysis of 41 human breast cancer cell lines reveals three new deleterious mutants. *Cancer Res.*, **66**, 41–45.
20. Mao,Z., Jiang,Y., Liu,X., Seluanov,A. and Gorbunova,V. (2009) DNA repair by homologous recombination, but not by nonhomologous end joining, is elevated in breast cancer cells. *Neoplasia*, **11**, 683–691.
21. Bennardo,N., Cheng,A., Huang,N. and Stark,J.M. (2008) Alternative-NHEJ is a mechanistically distinct pathway of mammalian chromosome break repair. *PLoS Genet.*, **4**, e1000110.
22. Abraham,K.J., Khosraviani,N., Chan,J.N.Y., Gorthi,A., Samman,A., Zhao,D.Y., Wang,M., Bokros,M., Vidya,E., Ostrowski,L.A. *et al.* (2020) Nucleolar RNA polymerase II drives ribosome biogenesis. *Nature*, **585**, 298–302.
23. Langmead,B. and Salzberg,S.L. (2012) Fast gapped-read alignment with Bowtie 2. *Nat. Methods*, **9**, 357–359.
24. Zhang,Y., Liu,T., Meyer,C.A., Eeckhoute,J., Johnson,D.S., Bernstein,B.E., Nusbaum,C., Myers,R.M., Brown,M., Li,W. *et al.* (2008) Model-based analysis of ChIP-Seq (MACS). *Genome Biol.*, **9**, R137.
25. Li,Q., Brown,J.B., Huang,H. and Bickel,P.J. and (2011) Measuring reproducibility of high-throughput experiments. *Ann. Appl. Stat.*, **5**, 1752–1779.
26. Ramirez,F., Ryan,D.P., Gruning,B., Bhardwaj,V., Kilpert,F., Richter,A.S., Heyne,S., Dundar,F. and Manke,T. (2016) deepTools2: a next generation web server for deep-sequencing data analysis. *Nucleic Acids Res.*, **44**, W160–W165.

27. Dobin,A., Davis,C.A., Schlesinger,F., Drenkow,J., Zaleski,C., Jha,S., Batut,P., Chaisson,M. and Gingeras,T.R. (2013) STAR: ultrafast universal RNA-seq aligner. *Bioinformatics*, **29**, 15–21.
28. Li,H., Handsaker,B., Wysoker,A., Fennell,T., Ruan,J., Homer,N., Marth,G., Abecasis,G., Durbin,R. and Genome Project Data Processing, S.Genome Project Data Processing, S. (2009) The sequence alignment/map format and SAMtools. *Bioinformatics*, **25**, 2078–2079.
29. Liao,Y., Smyth,G.K. and Shi,W. (2014) featureCounts: an efficient general purpose program for assigning sequence reads to genomic features. *Bioinformatics*, **30**, 923–930.
30. Tsai,L.J., Lopezcolorado,F.W., Bhargava,R., Mendez-Dorantes,C., Jahanshir,E. and Stark,J.M. (2020) RNF8 has both KU-dependent and independent roles in chromosomal break repair. *Nucleic Acids Res.*, **48**, 6032–6052.
31. Dine,J. and Deng,C.X. (2013) Mouse models of BRCA1 and their application to breast cancer research. *Cancer Metastasis Rev.*, **32**, 25–37.
32. Li,L., Guturi,K.K.N., Gautreau,B., Patel,P.S., Saad,A., Morii,M., Mateo,F., Palomero,L., Barbour,H., Gomez,A. *et al.* (2018) Ubiquitin ligase RNF8 suppresses Notch signaling to regulate mammary development and tumorigenesis. *J. Clin. Invest.*, **128**, 4525–4542.
33. Nik-Zainal,S., Alexandrov,L.B., Wedge,D.C., Van Loo,P., Greenman,C.D., Raine,K., Jones,D., Hinton,J., Marshall,J., Stebbings,L.A. *et al.* (2012) Mutational processes molding the genomes of 21 breast cancers. *Cell*, **149**, 979–993.
34. Alexandrov,L.B., Nik-Zainal,S., Wedge,D.C., Aparicio,S.A., Behjati,S., Biankin,A.V., Bignell,G.R., Bolli,N., Borg,A., Borresen-Dale,A.L. *et al.* (2013) Signatures of mutational processes in human cancer. *Nature*, **500**, 415–421.
35. Bryant,H.E., Schultz,N., Thomas,H.D., Parker,K.M., Flower,D., Lopez,E., Kyle,S., Meuth,M., Curtin,N.J. and Helleday,T. (2005) Specific killing of BRCA2-deficient tumours with inhibitors of poly(ADP-ribose) polymerase. *Nature*, **434**, 913–917.
36. Farmer,H., McCabe,N., Lord,C.J., Tutt,A.N., Johnson,D.A., Richardson,T.B., Santarosa,M., Dillon,K.J., Hickson,I., Knights,C. *et al.* (2005) Targeting the DNA repair defect in BRCA mutant cells as a therapeutic strategy. *Nature*, **434**, 917–921.
37. Panier,S. and Boulton,S.J. (2014) Double-strand break repair: 53BP1 comes into focus. *Nat. Rev. Mol. Cell Biol.*, **15**, 7–18.
38. Gorgoulis,V., Adams,P.D., Alimonti,A., Bennett,D.C., Bischof,O., Bishop,C., Campisi,J., Collado,M., Evangelou,K., Ferbeyre,G. *et al.* (2019) Cellular senescence: defining a path forward. *Cell*, **179**, 813–827.
39. Shanbhag,N.M., Rafalska-Metcalf,I.U., Balane-Bolivar,C., Janicki,S.M. and Greenberg,R.A. (2010) ATM-dependent chromatin changes silence transcription in cis to DNA double-strand breaks. *Cell*, **141**, 970–981.
40. Paul,A. and Wang,B. (2017) RNF8- and Ube2S-dependent ubiquitin lysine 11-linkage modification in response to DNA damage. *Mol. Cell*, **66**, 458–472.
41. Taglialatela,A., Alvarez,S., Leuzzi,G., Sannino,V., Ranjha,L., Huang,J.W., Madubata,C., Anand,R., Levy,B., Rabadan,R. *et al.* (2017) Restoration of replication fork stability in BRCA1- and BRCA2-deficient cells by inactivation of SNF2-Family fork remodelers. *Mol. Cell*, **68**, 414–430.
42. Hatchi,E., Skourti-Stathaki,K., Ventz,S., Pinello,L., Yen,A., Kamieniarz-Gdula,K., Dimitrov,S., Pathania,S., McKinney,K.M., Eaton,M.L. *et al.* (2015) BRCA1 recruitment to transcriptional pause sites is required for R-loop-driven DNA damage repair. *Mol. Cell*, **57**, 636–647.
43. Crossley,M.P., Brickner,J.R., Song,C., Zar,S.M.T., Maw,S.S., Chedin,F., Tsai,M.S. and Cimprich,K.A. (2021) Catalytically inactive, purified RNase H1: a specific and sensitive probe for RNA-DNA hybrid imaging. *J. Cell Biol.*, **220**, e202101092.
44. Crossley,M.P., Song,C., Bocek,M.J., Choi,J.H., Kousorous,J., Sathirachinda,A., Lin,C., Brickner,J.R., Bai,G., Lans,H. *et al.* (2023) R-loop-derived cytoplasmic RNA-DNA hybrids activate an immune response. *Nature*, **613**, 187–194.
45. Promonet,A., Padioleau,I., Liu,Y., Sanz,L., Biernacka,A., Schmitz,A.L., Skrzypczak,M., Sarrazin,A., Mettling,C., Rowicka,M. *et al.* (2020) Topoisomerase 1 prevents replication stress at R-loop-enriched transcription termination sites. *Nat. Commun.*, **11**, 3940.
46. Skourti-Stathaki,K., Proudfoot,N.J. and Gromak,N. (2011) Human senataxin resolves RNA/DNA hybrids formed at transcriptional pause sites to promote Xrn2-dependent termination. *Mol. Cell*, **42**, 794–805.
47. Lockhart,A., Pires,V.B., Bento,F., Kellner,V., Luke-Glaser,S., Yakoub,G., Ulrich,H.D. and Luke,B. (2019) RNase H1 and H2 are differentially regulated to process RNA-DNA hybrids. *Cell Rep.*, **29**, 2890–2900.
48. Patel,P.S., Abraham,K.J., Guturi,K.K.N., Halaby,M.J., Khan,Z., Palomero,L., Ho,B., Duan,S., St-Germain,J., Algouneh,A. *et al.* (2021) RNF168 regulates R-loop resolution and genomic stability in BRCA1/2-deficient tumors. *J. Clin. Invest.*, **131**, e140105.
49. Pineiro,D., Stoneley,M., Ramakrishna,M., Alexandrova,J., Dezi,V., Juke-Jones,R., Lilley,K.S., Cain,K. and Willis,A.E. (2018) Identification of the RNA polymerase I-RNA interactome. *Nucleic Acids Res.*, **46**, 11002–11013.
50. Gaillard,H., Garcia-Muse,T. and Aguilera,A. (2015) Replication stress and cancer. *Nat. Rev. Cancer*, **15**, 276–289.
51. Gan,W., Guan,Z., Liu,J., Gui,T., Shen,K., Manley,J.L. and Li,X. (2011) R-loop-mediated genomic instability is caused by impairment of replication fork progression. *Genes Dev.*, **25**, 2041–2056.
52. Hamperl,S., Bocek,M.J., Saldivar,J.C., Swigut,T. and Cimprich,K.A. (2017) Transcription-replication conflict orientation modulates R-loop levels and activates distinct DNA damage responses. *Cell*, **170**, 774–786.
53. Lang,K.S., Hall,A.N., Merrikh,C.N., Ragheb,M., Tabakh,H., Pollock,A.J., Woodward,J.J., Dreifus,J.E. and Merrikh,H. (2017) Replication-transcription conflicts generate R-loops that orchestrate bacterial stress survival and pathogenesis. *Cell*, **170**, 787–799.
54. Quinet,A., Carvajal-Maldonado,D., Lemacon,D. and Vindigni,A. (2017) DNA Fiber analysis: mind the gap.! *Methods Enzymol.*, **591**, 55–82.
55. Cristini,A., Groh,M., Kristiansen,M.S. and Gromak,N. (2018) RNA/DNA hybrid interactome identifies DXH9 as a molecular player in transcriptional termination and R-loop-associated DNA damage. *Cell Rep.*, **23**, 1891–1905.
56. Wang,I.X., Grunseich,C., Fox,J., Burdick,J., Zhu,Z., Ravazian,N., Hafner,M. and Cheung,V.G. (2018) Human proteins that interact with RNA/DNA hybrids. *Genome Res.*, **28**, 1405–1414.
57. Villarreal,O.D., Mersaoui,S.Y., Yu,Z., Masson,J.Y. and Richard,S. (2020) Genome-wide R-loop analysis defines unique roles for DDX5, XRN2, and PRMT5 in DNA/RNA hybrid resolution. *Life Sci. Alliance*, **3**, e202000762.
58. Brannan,K., Kim,H., Erickson,B., Glover-Cutter,K., Kim,S., Fong,N., Kiemele,L., Hansen,K., Davis,R., Lykke-Andersen,J. *et al.* (2012) mRNA decapping factors and the exonuclease Xrn2 function in widespread premature termination of RNA polymerase II transcription. *Mol. Cell*, **46**, 311–324.
59. Patel,P.S., Algouneh,A. and Hakem,R. (2021) Exploiting synthetic lethality to target BRCA1/2-deficient tumors: where we stand. *Oncogene*, **40**, 3001–3014.
60. Morales,J.C., Richard,P., Patidar,P.L., Motea,E.A., Dang,T.T., Manley,J.L. and Boothman,D.A. (2016) XRN2 Links transcription termination to DNA damage and replication stress. *PLoS Genet.*, **12**, e1006107.
61. Hasanova,Z., Klapstova,V., Porrua,O., Stefl,R. and Sebesta,M. (2023) Human senataxin is a bona fide R-loop resolving enzyme and transcription termination factor. *Nucleic Acids Res.*, **51**, 2818–2837.
62. Belotserkovskii,B.P., Tornaletti,S., D'Souza,A.D. and Hanawalt,P.C. (2018) R-loop generation during transcription: formation, processing and cellular outcomes. *DNA Repair (Amst.)*, **71**, 69–81.
63. Doil,C., Mailand,N., Bekker-Jensen,S., Menard,P., Larsen,D.H., Pepperkok,R., Ellenberg,J., Panier,S., Durocher,D., Bartek,J. *et al.* (2009) RNF168 binds and amplifies ubiquitin conjugates on damaged chromosomes to allow accumulation of repair proteins. *Cell*, **136**, 435–446.